From Particles to Flocs: Revealing Where Flocculation Occurs in the Nearfield of a Negatively-Buoyant River Plume in a Large Lake (Lake Geneva)

Violaine Piton, Ulrich Lemmin, François Bourrin, Htet Kyi Wynn, Valentin Kindschi, David Andrew Barry

JGR Oceans

RESEARCH ARTICLE
10.1029/2023JC019860

From Particles to Flocs: Revealing Where Flocculation Occurs in the Nearfield of a Negatively-Buoyant River Plume in a Large Lake (Lake Geneva)

Violaine Piton[1], Ulrich Lemmin[1], François Bourrin[2], Htet Kyi Wynn[1], Valentin Kindschi[1], and David Andrew Barry[1]

[1]Ecological Engineering Laboratory (ECOL), Environmental Engineering Institute (IIE), Faculty of Architecture, Civil and Environmental Engineering (ENAC), Ecole Polytechnique Fédérale de Lausanne (EPFL), Lausanne, Switzerland, [2]Centre de Formation et de Recherche sur les Environnements Méditerranéens, CNRS, UMR 5110, Université de Perpignan Via Domitia, Perpignan, France

Abstract The dynamics of sediments entering lakes in river plumes is virtually unknown. This field study provides unprecedented evidence of the initiation and evolution of suspended sediment flocculation in the nearfield of the negatively-buoyant Rhône River plume, flowing as interflow in the thermocline of stratified Lake Geneva. Sediment floc property changes (formation, size, composition, shape) with depth and distance from the mouth, were determined by combining digital holographic camera LISST-HOLO data with full-depth in situ profiles of particle size (LISST-100X), density, turbidity, currents and water samples taken along the plume path. The total suspended matter volume of inflowing Rhône River waters (~155 mg l^{-1}) mostly consisted of clays (<4 μm), very fine silts (4–8 μm) and small contributions of microflocs (20–100 μm). This composition was also found in the interflow plume core. Above the plume, in the epilimnion, fine silts, microflocs and numerous phytoplanktonic organisms (~200 μm) were observed, representative of the lake background. High levels of shear (15–27 s^{-1}) and turbulence occurred in the shear layer that formed between the interflow bottom and the hypolimnion below. It was found that macroflocs only formed in this shear layer. In the hypolimnion, sediment load was the lowest and macroflocs (up to ~300 μm) composed of inorganic particles were dominant. The size of the largest flocs was limited by the size of the smallest turbulent eddies determined by the Kolmogorov microscale. Floc 3D fractal dimensions of ~2.1–2.5 suggest an intermediate shape complexity between marine snow and sludge flocs.

Plain Language Summary Suspended sediments with potentially hazardous substances adsorbed to them can enter lakes via river inflow, and thus can significantly impact lake water quality. It is therefore essential to understand their dynamics and fate in order to optimize water management policies. Suspended sediment aggregation (flocculation) is a process that allows aggregated particles to settle faster than primary particles, thereby affecting transport, dispersion and flux of suspended particles. Flocculation of suspended sediments is well documented in fluvial, estuarine and marine environments, but has rarely been investigated in lakes. In a new approach based on holographic camera images and water samples, this study, carried out in Lake Geneva, describes for the first time, the formation and evolution of large aggregates of sediments (flocs) along a river plume pathway in a large lake. Turbulence measurement revealed that a sufficient level of shear enhances floc formation in the shear layer at the bottom boundary of the plume, while the smallest turbulent eddies limit floc size. This knowledge is crucial, since it determines how sediment particles will spread or be deposited. Furthermore, our findings demonstrate that results from marine systems and estuaries cannot be directly applied to river plume interflows in lakes.

Key Points:

- Unprecedented evidence of initiation/evolution of suspended sediment flocculation in a river plume interflow nearfield in a lake is provided
- In the nearfield, all along the interflow path, macroflocs only formed in the shear layer between the interflow and the hypolimnion below
- Kolmogorov microscale limits macrofloc size, floc 3D fractal dimensions suggest a shape complexity between marine snow and sludge flocs

Supporting Information:

Supporting Information may be found in the online version of this article.

Correspondence to:

V. Piton,
violaine.piton@epfl.ch;
vpiton@mercator-ocean.fr

Citation:

Piton, V., Lemmin, U., Bourrin, F., Wynn, H. K., Kindschi, V., & Barry, D. A. (2024). From particles to flocs: Revealing where flocculation occurs in the nearfield of a negatively-buoyant river plume in a large lake (Lake Geneva). *Journal of Geophysical Research: Oceans*, *129*, e2023JC019860. https://doi.org/10.1029/2023JC019860

Received 27 MAR 2023
Accepted 9 JAN 2024

Author Contributions:

Conceptualization: Violaine Piton, Ulrich Lemmin, David Andrew Barry
Formal analysis: Violaine Piton
Methodology: Violaine Piton, Ulrich Lemmin
Resources: François Bourrin, Htet Kyi Wynn, Valentin Kindschi
Supervision: Ulrich Lemmin, David Andrew Barry
Visualization: Violaine Piton
Writing – original draft: Violaine Piton
Writing – review & editing: Ulrich Lemmin, François Bourrin, David Andrew Barry

1. Introduction

Suspended particle flocculation, or aggregation of primary particles (mainly clays and silts), is a complex process that controls the fate of suspended particles, as well as that of potentially hazardous substances adsorbed to them (Droppo et al., 1997; O'Connor, 1988; O'Melia & Tiller, 1993). For particles brought into a lake by river inflow, flocculation has important consequences for particle settling and the accumulation of sediment on the bed because: (a) the smallest primary particles can remain in suspension almost indefinitely and can be transported over great distances (Ishiguro & Balvay, 2003), or (b) these particles can rapidly settle to the lake bottom in the nearfield of the river plume, if they collide and become part of large porous flocs. In that case, they may create

local ecological hotspots, since studies globally indicate that settling velocities of flocs are an order of magnitude or more greater than settling velocities of primary disparate particles (e.g., Liu et al., 2022; Livsey et al., 2022). The nearfield of river plumes in lakes refers to the first one to two km from the river mouth. It is characterized by a flow field whose mean core velocity and velocity profiles rapidly change with distance from the river mouth, due to strong, unconfined spreading and intense mixing caused by entrainment. Thus, nearfield plume dynamics are dominated by shear and advection (e.g., Hetland, 2010; Piton et al., 2022). These changes can affect flocculation along the interflow path. Understanding flocculation dynamics of the Suspended Particulate Matter (SPM) in the nearfield, therefore, is key to maintaining good lake water quality and for developing effective lake management concepts. Yet, at present, little is known about flocculation dynamics in lakes, in particular, in the nearfield of river plumes.

Flocculation is controlled by a combination of physical, chemical and biological parameters such as particle concentration, turbulence, Brownian motion, differential settling, organic matter and salinity (Deng et al., 2022; Fugate & Friedrichs, 2003; Mehta, 2022; Pejrup & Mikkelsen, 2010; Tran & Strom, 2017). Salinity is often considered to be a factor affecting flocculation in estuarine and marine environments, whereas organic matter content and turbulence strongly influence freshwater flocculation (Droppo et al., 1998; Woodward & Walling, 2007). Biological activity affects the properties of flocs (structure, density, sedimentation rate and composition) due to the interaction between mineral clay particles, microorganisms and their excreted polymers (Extra Polymeric Substances (EPS); Deng et al., 2022). Over the years, floc formation dynamics has been investigated using different methods in field measurements, laboratory flume studies and oscillating grid experiments, mainly under uniform flow or steady state conditions (Fettweis et al., 2019; Gregory, 2013; Jarvis, Jefferson, & Parsons, 2005).

Turbulence first initiates and then enhances aggregation by increasing the collision frequency between particles (Hill et al., 1998; Kuprenas et al., 2018). Turbulence can also lead to floc disaggregation by fragmenting them into pieces of similar sizes, or by generating shear stresses that erode floc surfaces, thereby limiting their size to the same order of magnitude as the smallest turbulent eddies (Curran et al., 2007; Jarvis, Jefferson, Gregory, & Parsons, 2005; van Leussen, 1997). At low and intermediate turbulence rates, the emergence of a peak may occur in the observed floc size range, due to settling and residence time limits of large flocs (Mietta et al., 2009; Winterwerp, 1998; Zhang et al., 2022). At high turbulence rates, floc size decreases with an increase in shear rate (Dyer, 1989). Experiments show that floc strength increases with decreasing floc size (Jarvis, Jefferson, Gregory, & Parsons, 2005). However, floc formation and breakup also depend on floc internal composition, bonding, repulsive forces and shape.

Flocculation can form flocculi that range from a few microns, to microflocs of tens of microns, and to macroflocs of hundreds of microns (Lee et al., 2014). Microflocs are small, dense, quasi-spherical and resistant to turbulent mixing. Suggested maximum sizes range from 100 (Lafite, 1990) to 160 μm (Manning & Dyer, 1999). Under favorable conditions, microflocs collide with each other, flocculate and form larger aggregates referred to as macroflocs that are characterized by lower density and larger sizes of up to several millimeters (Eisma, 1993; Manning et al., 2004). Macroflocs have low cohesive strength, are porous and can be fragmented by shear forces (Jarvis, Jefferson, Gregory, & Parsons, 2005; Kranenburg, 1999). In laboratory experiments, the formation of macroflocs from the primary particles stage occurs within 50 min under favorable conditions (Chakraborti, 2005). Winterwerp (1999) indicated that flocs could only attain their equilibrium size if the residence time of the flocs is sufficiently long (order of hours).

Flocculation is well documented in fluvial (e.g., de Boer et al., 2000; Droppo & Ongley, 1992; Osborn et al., 2023; Slattery & Burt, 1997), estuarine (e.g., Gratiot et al., 2017; Verney et al., 2009; Winterwerp, 2002) and marine environments (e.g., Franck, 1973; Li et al., 2004; Many et al., 2016) mainly under steady flow conditions. Flocculation, however, has rarely been investigated in lakes. Laboratory experiments using suspended sediments from Lake Erie showed that the equilibrium time required for flocculation to occur under various shear stress and sediment concentration conditions is of O(1 hr) (Tsai et al., 1987). The largest flocs (median diameter ∼80–100 μm) were obtained when particle concentrations were the lowest (50–100 mg l^{-1}), whereas the highest concentrations (400–800 mg l^{-1}) led to formation of flocs with smaller median diameters (∼20–40 μm). Furthermore, floc size decreased from 100 to 50 μm when the shear stress increased from 0.1 to 0.4 Pa. Lick et al. (1993) found that flocs of untreated lake sediments were larger than flocs of sediments whose organic material was removed. There appear to only be two in situ studies dedicated to flocculation in lacustrine

environments. Using microscopy, Hodder and Gilbert (2007) reported that clastic suspended sediment in Lillooet Lake (Canada) is flocculated, with macroflocs (up to 280 μm) being mainly detected in the hypolimnion, where sediment loads were lowest. The sediment flux attributed to these macroflocs was equivalent to one-quarter of the average annual sediment flux (Hodder, 2009).

In Lake Geneva, flocculation dynamics are of particular interest in the nearfield of the negatively-buoyant plume of the Rhône River, because it is the main contributor to lake sediment content (~68% of the total particulate matter input). The Rhône River plume flows as an interflow at the thermocline depth during stratification (Figure 2; Giovannoli, 1990; Soulignac et al., 2021; Piton et al., 2022). Due to entrainment and sediment settling, SPM concentrations in the Rhône River plume decrease by a factor of 2–3 within 1,500 m from the river mouth; the interflow waters mostly contain fine particles <32 μm on the longest axis (Piton et al., 2022). These particles were transported 1,500 m from the mouth in the present study, and even far beyond (Ishiguro & Balvay, 2003). Piton et al. (2022) observed larger particles (>63 μm) below the interflow that could be expected to settle out in the nearfield area. However, they were not able to determine the nature of these large particles.

The objective of the present study is to establish whether these larger particles (>63 μm) are fine sands or flocs and whether and where flocculation occurs in the water column and along an unconfined river plume interflow pathway in the nearfield zone. Such a field investigation has not been carried out in a lake before. Based on unique simultaneous high-resolution field measurements of currents and turbulence, particle size distribution (PSD), particle images and water samples, the present study will address the following questions:

- Can SPM size, shape and composition be characterized along the water column in the nearfield of the Rhône River plume interflow in Lake Geneva?
- Does flocculation occur in the nearfield of the Rhône River interflow plume? If so, is there a preferential layer within the water column where this occurs?
- Do flocculation dynamics change along the Rhône River interflow pathway with distance from the river mouth?
- Can the processes enhancing and controlling flocculation be identified?

Figures, tables, and text with prefix S provide details and clarifications on certain topics discussed in the main text, and are found in Supporting Information S1.

2. Study Site

2.1. Lake Geneva

Lake Geneva (*Lac Léman*), situated between Switzerland and France, is Western Europe's largest lake (Figure 1a). This perialpine, warm, deep, oligomictic lake has a surface area of 582 km^2, a volume of 89 km^3 and a maximum depth of 309 m. The lake is thermally stratified from spring to early fall, with surface temperatures reaching up to 25°C. The thermocline (metalimnion) is located at ~15-m depth in summer and deepens during fall and winter. Occasionally, complete mixing takes place during very cold winters (CIPEL, 2019).

2.2. Rhône River

The Rhône River is a glacier-fed river, ~140 km long and has more than 20 short tributaries that also originate in glaciers. Its source is located at an altitude of ~2,200 m and the river descends down to an altitude of 370 m where it enters Lake Geneva (Figure 1b) as a 120-m wide channel (average depth 5 m). Since the Rhône River is considered a small river (Kelvin numbers range from 0.02 to 0.05), the nearfield plume is not affected by Coriolis force (Soulignac et al., 2021). It is the principal source of water and sediments for the lake, accounting for ~68% of the total water discharge and particulate matter input (Burkard, 1984; Zahner & Vernet, 1984).

At station Porte du Scex located 5 km upstream of the river mouth (Figure 1a), the Swiss Federal Office for the Environment (FOEN) continuously records discharge and turbidity, and also collects suspended sediment concentration (SSC) samples twice a week. We carried out a calibration between the SSC and the turbidity data over a 5-year period (2017–2021; linear regression $r = 0.91$; not shown) to convert the continuous turbidity data into continuous SSC.

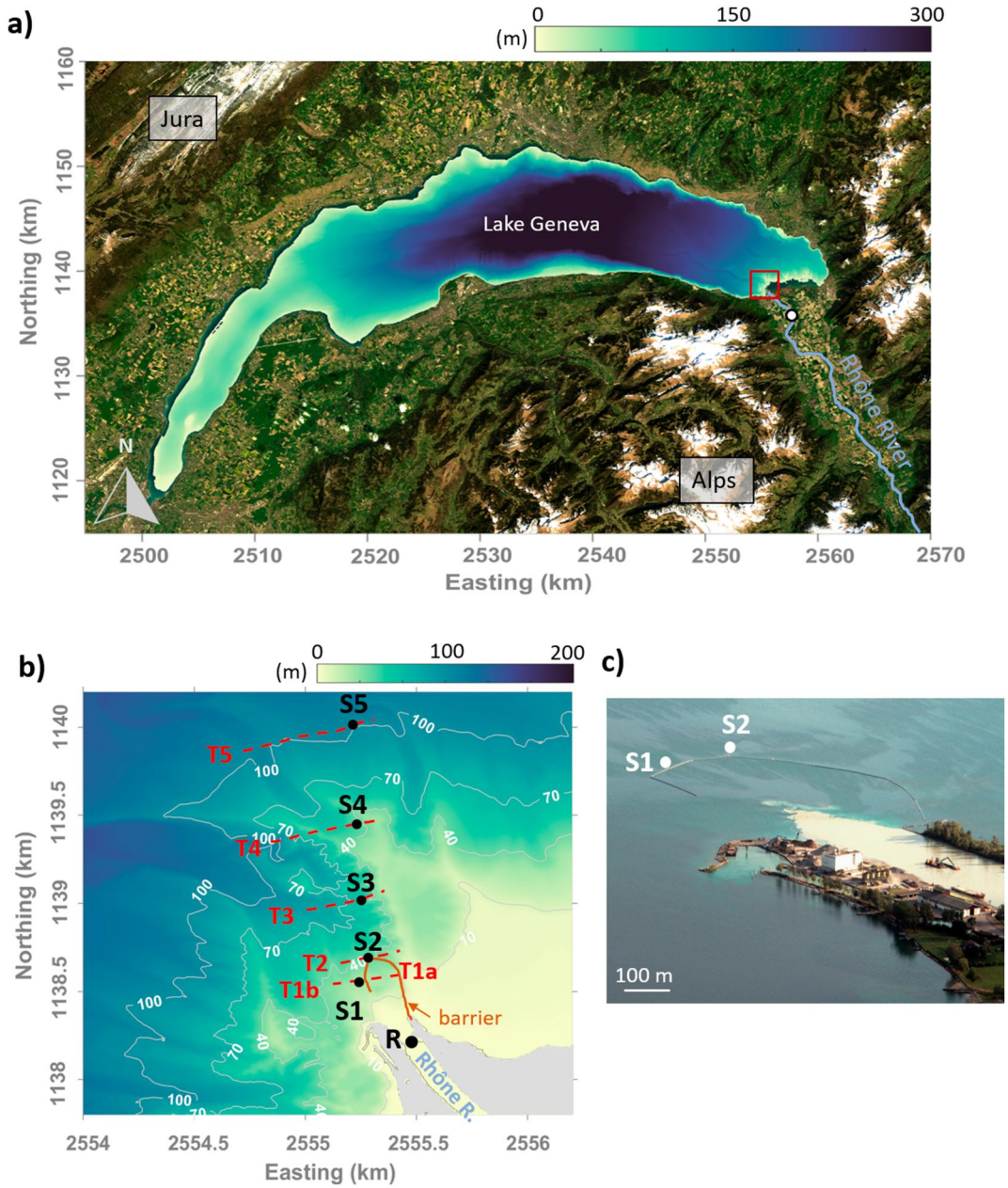

Figure 1. (a) Bathymetric map of Lake Geneva surrounded by the mountain chains, Jura and Alps. The FOEN hydrological survey station at Porte de Scex on the Rhône River is marked by a white circle. Small red box: study site located in front of Rhône River mouth. (b) Zoom of the study site where the Rhône River enters the lake. Black dots: stations S1, S2, S3, S4, and S5 where profile measurements were made. Black dot R: station in the Rhône River channel where water samples and LISST-100X measurements were taken. Red dashed lines: Acoustic Doppler Current Profiler transects T1a, T1b, T2, T3, T4, and T5. A floating barrier, traced in brown, retains driftwood that is periodically removed. Some depth contours (m) are given. (c) Representative aerial view of the Rhône River plume entering Lake Geneva. The plume is light colored due to its high sediment load. Progressive unconfined plunging occurs shortly after the plume enters the lake and results in a triangular plume shape. Stations S1 and S2 are indicated by the white dots. The Swiss coordinate system (CH1903+) is used (Swiss Federal Office of Topography, http://www.swisstopo.admin.ch, last accessed 7 March 2023). Colorbars indicate water depth.

The annual mean Rhône River discharge for 1970–2021 was 185 $m^3 s^{-1}$ with a mean SSC of 232 mg l^{-1}. The high flow season, with a mean water discharge of 245 $m^3 s^{-1}$ and an SSC of 410 mg l^{-1}, starts in May after snowmelt and lasts until the beginning of high-altitude freeze-up in October.

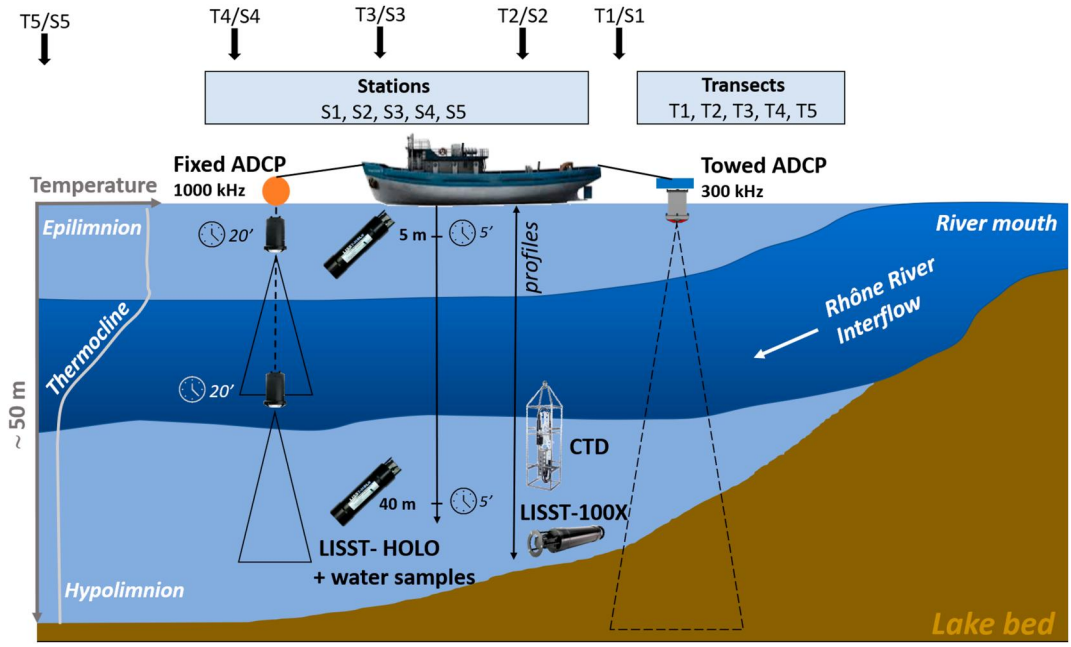

Figure 2. Schematic of measurement layout. Transect measurements were made with a towed Acoustic Doppler Current Profiler (ADCP, shown on the right side). Water column measurements at stations in the center of the transects (shown on the left side) consisted of taking Conductivity Temperature Depth (CTD) and LISST 100X profiles, LISST-HOLO measurements at 5 and 40 m depth and Nortek signature ADCP profiles with the instrument suspended from a buoy. The interflow layer of the river plume is marked in dark blue; its depth is determined by the thermal stratification in the lake (temperature profile on the left, gray line). Black arrows on top indicate the approximate position of the transects/stations along the interflow. For transect and station locations, see also Figure 1b.

3. Methods

3.1. Measurement Campaigns

Field campaigns were conducted in September 2021 in front of the river mouth at high river discharge (~300 m^3 s^{-1}) during the stratified period when interflow is well developed, in order to investigate the SPM variability along the Rhône interflow pathway (Figures 1 and 2). Five stations (S1-S5, Figures 1b and 2) were sampled on 14 September 2021. Stations S2-S5 were on the interflow pathway. Their locations were determined from high resolution Acoustic Doppler Current Profiler (ADCP) transects T1-T5 (Figure 1b) measured prior to each station sampling (Piton et al., 2022; Soulignac et al., 2021). A 300-kHz Teledyne Marine Workhorse Sentinel in Mode 12 was used, with high-rate pinging, beam bins of 1-m height at 1 Hz, and in high-resolution bottom-tracking mode. The received level of the acoustic return signal along each beam of the ADCP was converted into the Backscattering Index BI (Text S1 in Supporting Information S1). The maximum intensity of ADCP BI was taken as the interflow center (Figure S1 in Supporting Information S1). Due to strong currents in the river plunge region (Figure 1c), station S1 was located slightly to the left of the main inflow trajectory (Figure 1b). An additional station, R, located in the Rhône River (Figure 1b), was selected to measure river sediment properties.

3.2. Water Column Sampling Instrumentation

At each of the five stations S1–S5, additional time series of velocity profiles were obtained from a buoy-mounted, downward-looking five-beam acoustic profiler Nortek Signature1000 (kHz) ADCP (Figure 2). The instrument was configured to measure current intensities/directions in along-beam bins of 0.2-m height at 8 Hz. The blanking distance was 0.1 m and the vertical range was 18.8 m. This configuration allows resolving turbulence scales. To cover the whole vertical extent of the interflow, the instrument was first deployed for 20 min at 6.5 m below the surface and then for another 20 min at 26 m below the surface, thus providing depth profiles ranging from 6.6 to 44.9-m depth.

In parallel to Signature1000 measurements, vertical profiles of Conductivity, Temperature, Depth (CTD) and turbidity (at 0.3 Hz) were collected at stations S1-S5 (Figure 1b) with a multiparameter probe (Sea & Sun Marine Tech CTD 75M), equipped with an optical turbidity sensor (Sea Point Inc.). Depth profiles of PSD and concentration were measured using an in situ laser scattering and transmissometry instrument (Sequoia Scientific LISST-100X, type C, size range from 2.25 to 350 µm, sampling rate 1 Hz; Text S3 in Supporting Information S1) (Figure 2). The instrument and its operation principles are described in Agrawal and Pottsmith (2000). Uncertainties in LISST measurements may arise in the case of non-spherical particles, flocs exceeding the measurable range, SSC values that are too high, stratification of the water column and/or multiple scattering (Agrawal & Pottsmith, 2000). LISST measurements of large size particles may be affected by schlieren, which is produced by light scattering resulting from density differences. Density fluctuations occur in strong density gradient regions in the thermocline or in shear layers with high turbulence (Mikkelsen et al., 2008; Styles, 2006). Andrews et al. (2010) determined that the inorganic matrix will still function adequately for particles covering a wide range of shapes and composition. Due to the uncertainties, it is suggested that the results of LISST measurements can be interpreted as an index for comparing size distributions rather than relying on their exact values (Fettweis, 2008; Fugate & Friedrichs, 2003). The LISST data will be interpreted in this manner in the present study.

It was pointed out that accurate independent measurements of aggregate sizes and shapes may best be made with video and still photographic techniques (e.g., Graham & Nimmo-Smith, 2010; Graham et al., 2012; Manning et al., 2004; Mikkelsen et al., 2006; Osborn et al., 2021; Wheatland et al., 2020). Therefore, in order to study the volume, number and shape of large particles, a digital holographic camera (Sequoia Scientific, LISST-HOLO, 30–2,000 µm, 0.2 Hz; 4.4 µm pixel size digital camera; 1,600 × 1,200 pixels) was also deployed. For imaging small objects, holography offers a good alternative that can overcome the limitations of focal plane photography of video or still camera systems. Due to its concentration limit (maximum ∼50 mg l^{-1}), no measurements were carried out in the interflow plume given the higher SPM concentrations. At each station, measurements were taken for 5 min to collect statistically significant data at two depths: one at ∼5 m depth (above the interflow) and a second one at ∼40 m depth (below the interflow) (Figure 2). During each measurement series, ∼60 images were obtained. Water samples were collected with a Niskin bottle at these two depths for each station. An additional water sample was collected at 20 m, in the interflow core, at station S5.

3.3. Rhône River Sampling

The PSD and concentration of the Rhône River water were estimated from 2-min averages of LISST-100X measurements taken at station R at ∼0.5 m depth (Figure 1b). The instrument was equipped with a 90% path reduction module. A water sample was collected at the same depth.

3.4. Turbulence

Signature1000 ADCP data were quality controlled to remove measurements with low beam correlation (<50) and low echo amplitude (<30 dB) following manufacturer recommendations. For each bin (0.2-m high) of the time series, the Turbulent Kinetic Energy (TKE) dissipation rate ε was estimated from frequency spectra S (Lumley & Terray, 1983) (Figure S2 in Supporting Information S1). A region of isotropic turbulence is present at mid-frequencies ($0.4 < f < 2$ Hz), which follows the classic $f^{-5/3}$ energy cascade (Kolmogorov, 1941) (Figure S2 in Supporting Information S1). From the TKE frequency spectrum S, the dissipation rate ε was computed within each bin as:

$$S(f) = \alpha \varepsilon^{2/3} f^{-5/3} \left(\frac{\overline{v}}{2\pi}\right)^{2/3} \quad (1)$$

where α is a constant equal to 0.69 (Sreenivasan, 1995), f is the frequency and $\overline{v}$ is the mean normal velocity. Further details on this approach and the associated Matlab codes are given in Guerra and Thomson (2017).

The following two parameters, expressed in terms of the energy dissipation rate, ε, are used to analyze flocculation dependence on turbulence: the Kolmogorov turbulent microscale λ_k (in µm)

$$\lambda_k = \left(\frac{\nu^3}{\varepsilon}\right)^{1/4} \quad (2)$$

and the shear rate Γ (in s^{-1})

$$\Gamma = \left(\frac{\varepsilon}{\nu}\right)^{1/2} \quad (3)$$

where ν is the molecular viscosity; λ_k is used as an indicator of effective aggregate size (Fugate & Friedrichs, 2003), and Γ is a quantitative measure of turbulent mixing (Kuprenas et al., 2018; Strom & Keyvani, 2016).

3.5. Suspended Matter Properties

3.5.1. SPM Concentration From Water Samples

SPM concentrations were determined from the water samples by filtering (see Text S2 in Supporting Information S1 for details).

3.5.2. Calibration of Optical Turbidity

The turbidity sensor mounted on the CTD gives turbidity in Formarzin Turbidity Units. Measurements were calibrated against gravimetric SPM concentration measurements (SPM_{Filter}, Text S2 in Supporting Information S1). Optical turbidity is a complex analytical parameter that is affected by Inherent Optical Properties of particles. Although optical sensors are primarily affected by SPM concentrations, factors such as individual particle size, particle shape, sediment color and degree of flocculation/disaggregation also influence sensor response. Optical backscattering sensors were found to be suitable tools for sediment studies (e.g., Bowers et al., 2017; Druine et al., 2018). It is generally accepted that a linear regression between turbidity and SPM is acceptable, if the regression coefficient is >90% (Fettweis et al., 2019; Rasmussen et al., 2009; Sehgal et al., 2022). The regression line ($r = 0.98$) between the optical turbidity and the filtered SPM_{Filter} concentration (in mg l^{-1}) has a slope of $a = 1.1$ and an intercept of $b = 3.08$. Based on this relationship, SPM_{OPT}, which corresponds to the calibrated SPM concentrations derived from the optical measurements (turbidity), was determined from the turbidity profiles for each station.

3.5.3. In Situ Particle Size Distribution

Particle properties, the SPM Volume Concentration (Suspended Particulate Matter Volume Concentration (SPMVC)), PSD and the diameter corresponding to 50% of the cumulative volume concentration (D_{50}) were derived from LISST-100X profile measurements. For details, see Text S3 in Supporting Information S1.

3.5.4. In Situ Particle Shape Distribution

The LISST-HOLO was used to study the volume, number and shape of large particles, complex aggregates and biological organisms within the range 30–2,000 µm (Graham & Nimmo-Smith, 2010). Data analysis provided the particle Equivalent Circular Diameter (ECD, in µm), the particle perimeter (P, in µm), the particle area (A, in μm^2) and the minor and major axes of the particle (Ax_{min} and Ax_{maj}, respectively, in µm). The perimeter-based fractal dimension (DF) was computed as (Maggi & Winterwerp, 2004; Vahedi & Gorczyca, 2011):

$$DF = 2\frac{\log(P)}{\log(A)} \quad (4)$$

Further details are provided in Text S4 of Supporting Information S1.

3.5.5. Laboratory Particle Size Distribution

In the laboratory, the water samples were deflocculated and the deflocculated PSD was estimated (details in Text S5 of Supporting Information S1).

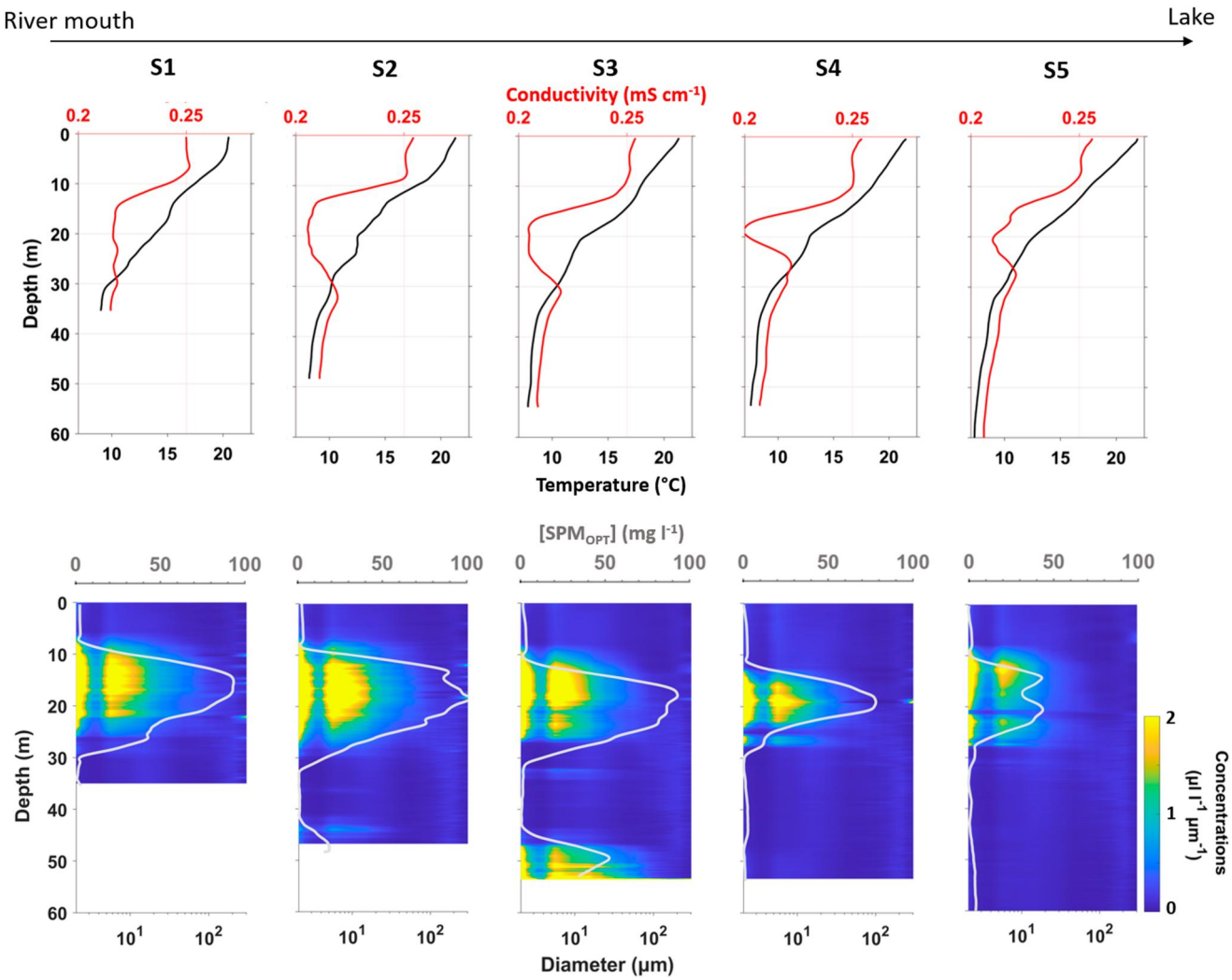

Figure 3. For the five stations S1–S5 along the interflow plume. Top panels: profiles of temperature (black lines) and electrical conductivity at 25°C (red lines). Bottom panels: SPM_{OPT} profiles (gray lines) plotted over concentration profiles of particles per size class (color maps, from LISST-100X). The colorbar gives the (volume) particle concentration per size class (µl l^{-1} $µm^{-1}$). At each station, profiles are shown to the lake bed. For station locations, see Figure 1b.

4. Results

4.1. Environmental Conditions

Results from the campaign carried out on 14 September 2021 will be discussed below. A preliminary campaign on 9 September 2021 under comparable conditions gave similar results (not shown). On 14 September 2021, the wind was low (<3 m s^{-1}) and blew southeastward in the morning and northwestward in the afternoon (Figure S3 in Supporting Information S1). The Rhône River discharge and the SSC evolved similarly during the day, with mean values of 254 m^3 s^{-1} and 155 mg l^{-1}, respectively. The average discharge was close to the seasonal mean (245 m^3 s^{-1}), whereas the mean SSC was lower than the seasonal mean (410 mg l^{-1}).

Profiles of temperature and conductivity show weak stratification, which is typical for the beginning of the cooling season. The metalimnion was located between ~5 and ~30-m depth, with temperature decreasing from 21°C near the surface to 9°C below 30-m depth (Figure 3). Conductivity dropped from 0.25 near the surface to a minimum of 0.20 mS cm^{-1} at ~20-m depth. Low conductivity values are characteristic for Rhône River waters, which permits tracing the depth of the Rhône River interflow.

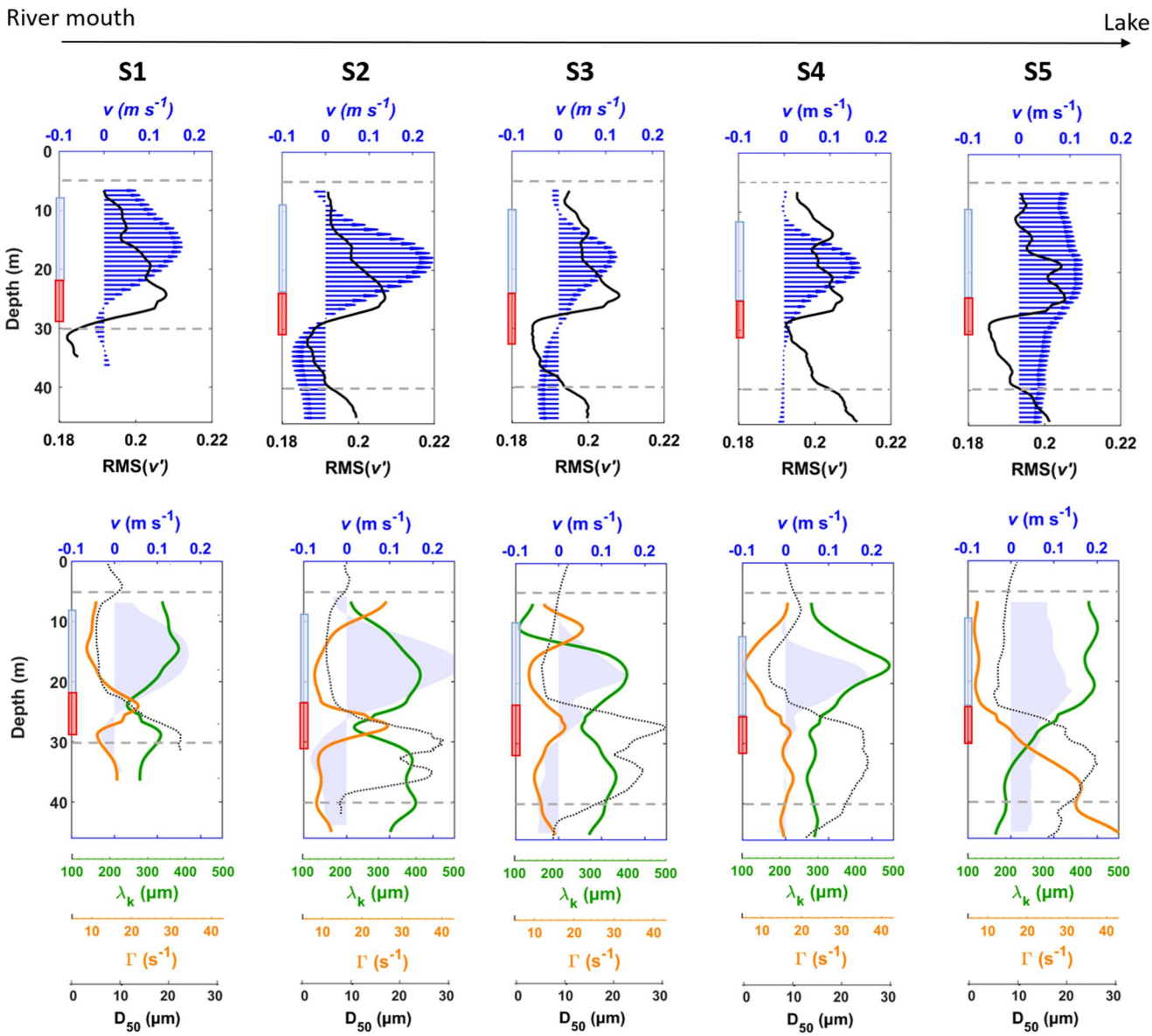

Figure 4. For stations S1–S5. Top panels: vertical profiles of normal velocity (v; blue arrows) measured by the Teledyne Acoustic Doppler Current Profiler and of RMS (v') (black lines) obtained from Nortek Signature data for each station. Bottom panels: vertical profiles of the Kolmogorov turbulent microscale, λ_k (green lines), and the shear rate, Γ (orange lines) obtained from Signature data, and D_{50} of the sediment (gray lines). In the lower panels, normal velocity profiles shown in the top panels are shaded in blue. The depth range of the jet-like normal velocity profile in the interflow is marked by a light blue bar on the left vertical axis in each panel. The red bars indicate the shear layer range. Horizontal black dashed lines: depths 5-, 30-, and 40-m where the particle size distributions will be further detailed with LISST-HOLO measurements. For station locations, see Figures 1b and 2.

4.2. Hydrodynamics

4.2.1. Mean Flow Patterns

At stations S1-S4, vertical profiles of the normal (northward) current (v) derived from the full-depth ADCP profile measurements show sharp, jet-like, symmetrical tapering above and below the maximum that reaches up to 0.25 m s^{-1} (Figure 4), which is centered in the layer where low conductivity values indicate the Rhône River inflow (Figure 3). Above 10 m depth (S2–S4) and below 25 m depth (S1–S4), small currents flow southward. This confirms that the Rhône River plume had developed into an interflow. It spreads laterally unconfined within the thermocline from ∼10 to 25 m depth (Figure 3), and flows northward, straight out from the river channel (Figure 1b). This plume pattern agrees with the one that was previously observed (Piton et al., 2022; Soulignac

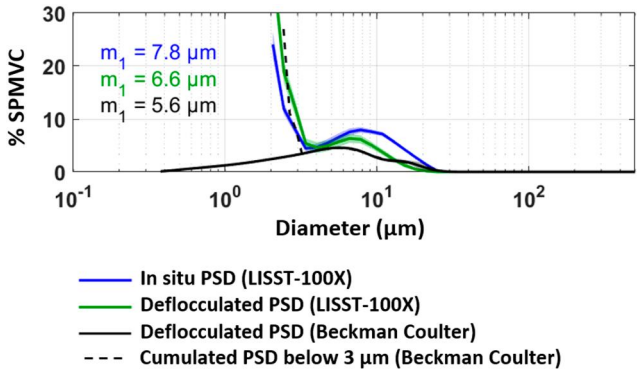

Figure 5. Particle size distribution (% of total Suspended Particulate Matter Volume Concentration (SPMVC) for size classes in µm) at station R at 0.5-m depth in the Rhône River (for location, see Figure 1b) derived from: direct in situ measurements with the LISST-100X (blue line), a deflocculated water sample measured with the LISST-100X (green line), and a deflocculated water sample measured with the Beckman Coulter (black line). The black dashed line corresponds to the cumulated proportions of particles below 3 µm measured by the Beckman Coulter, and m_1 gives the median size for each curve.

et al., 2021). The velocity profile slightly differs at S1 since the interflow is not yet fully established at that distance from the mouth (350 m). The jet-like profile becomes less evident at S5, which is located furthest away from the mouth.

At each station, profiles of the Root Mean Square velocity fluctuations in the streamwise (normal) direction, RMS(v'), derived from Signature1000 profiles show values progressively increasing from 8 to ~25 m depth, where they reach a maximum value of ~0.2 m s^{-1} (Figure 4). A strong decrease of RMS (v') occurs between 25 and 30 m depth, while below 30 m, the values progressively increase again toward the bottom of the profiles.

4.2.2. Turbulence Patterns

At stations S2-S4, profiles of shear rate Γ exhibit peaks in the upper (~8–10 m) and lower (~25–30-m depth) boundaries of the interflow where horizontal velocity strongly changes from high velocities in the interflow to low velocities in the ambient waters (Figure 4), suggesting that intense turbulent mixing occurs in the boundary layers between the interflow waters and the ambient lake waters due to shear; thus these boundaries are shear layers. Within the core of the interflow (~10–20 m depth), Γ values are low, indicating weak mixing. Below 30 m depth, Γ remains low and almost constant down to the bottom of the profiles. Profiles of Γ at stations S1 and S5 are homogeneous from 8 to 20 m depth, because the upper boundary of the interflow is not well defined; it is not yet formed at S1 and is already well mixed with ambient waters at S5, in agreement with the normal velocity profiles (Figure 4 top panels).

The shape of profiles of the Kolmogorov turbulent microscale λ_k is inverse to that of profiles of Γ as expected from Equations 2 and 3. Highest values of λ_k (~350–500 µm) are found within the core of the interflow between ~10 and ~20 m depth (Figure 4), while lower values (~200–300 µm) are observed in the shear layers in the upper and lower boundaries of the interflow.

4.3. SPM Properties

4.3.1. In the Rhône River

The PSD spectrum derived from direct in situ measurements performed at station R (Figure 1b) with the LISST-100X shows a unimodal distribution with a mode at 7.8 µm (blue line in Figure 5). Note that the high value for particles <3 µm is not considered as a mode, but rather as an indication of the presence of very fine particles. Note that concentrations below the detection limit of the LISST-100X (2.25 µm) cause increased concentrations of the two smallest size classes (Fettweis & Baeye, 2015; Graham et al., 2012).

A water sample was collected at the same time and depth. The Particulate Organic Matter content (POM) of the total SPM was below 1.5% (Table S1 in Supporting Information S1). The deflocculated PSD measured by the LISST-100X in the laboratory after sample treatment (Text S5 in Supporting Information S1) presents a unimodal distribution with a mode at 6.6 µm, and with a reduced contribution of particles 10–20 µm to the total SPMVC compared to the in situ measurement (green line in Figure 5). This suggests that some particles in the 10–20 µm range observed in situ were microflocs. Similarly, the deflocculated PSD measured by the Beckman Coulter is unimodal with a mode at 5.6 µm (black line in Figure 5). The slight discrepancies in the mode of the two deflocculated PSDs are probably due to the different sensitivities of the two instruments. The deflocculated PSD from the Beckman Coulter allows to detail the fine particle distribution below ~3 µm, which is below the detection limit of the LISST-100X, and shows the presence of primary particles as small as 0.5 µm. When cumulated, the contribution of particles <3 µm (black dashed line in Figure 5) coincides with the contributions of particles <3 µm measured by the LISST-100X (green line in Figure 5).

These results suggest that based on the Udden-Wentworth grain-size scale (Udden, 1914; Wentworth, 1922), the Rhône River waters carry fine cohesive particles such as clays (0.5–4 µm), very fine silts (4–8 µm) and fine silts (8–15 µm), with a limited contribution of organic matter, but do not carry large particles (sands).

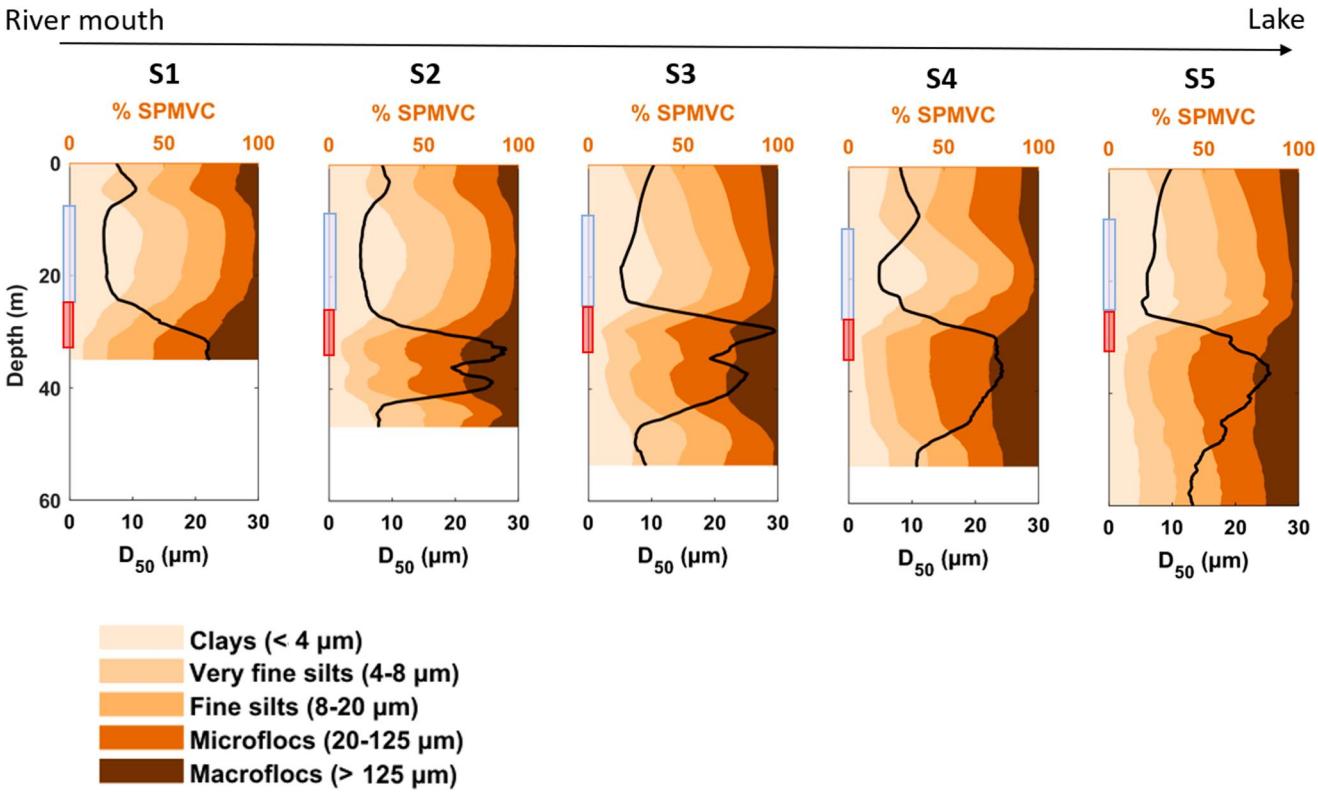

Figure 6. For stations S1–S5: Profiles of D_{50} (μm; black line) derived from the LISST-100X measurements for each station, superimposed on profiles of corresponding proportions of clays, very fine silts, fine silts, microflocs and macroflocs in terms of % of Suspended Particulate Matter Volume Concentration (SPMVC). All profiles are shown to the local maximum depth. The depth range of the jet-like normal velocity profile in the interflow (Figure 3) is marked by a light blue bar on the left vertical axis in each panel. The red bars indicate the shear layer range. The legend gives the particle size classes. For station locations, see Figures 1b and 2.

4.3.2. Along the Interflow Pathway

The profiles of normalized particle concentration per size class, measured with the LISST-100X at each station (Figure 6), contained high concentrations for particle diameters in the range 2–20 μm (clay to fine silts) at depths where conductivity was lowest (Figure 3) and normal velocities were highest (Figure 4), indicating that highest particle concentrations are carried in the core of the Rhône River interflow. At ∼15 m depth for stations S1–S3 and at ∼20-m depth for S4 and S5, the concentrations were highest (>2 μl l^{-1} μm^{-1}) for particles <3 μm and for particles in the range 6–10 μm. The corresponding D_{50} profiles show values <8 μm in that depth range (Figure 6). This suggests that the interflow waters mainly carried fine particles. Profiles of SPM_{OPT} obtained from CTD turbidity profiles also show large values in the highly particle-laden interflow depth range (Figure 3), with values up to 100 mg l^{-1} at S2.

The maximum value in the interflow depth range progressively decreases with distance from the mouth, down to 45 mg l^{-1} at S5. At the same time, below the interflow, concentrations ∼0.3 μl l^{-1} μm^{-1} were measured for particle diameters >100 μm from 30 m depth down to the bottom of the water column from stations S2 to S5 (Figure 3). A similar pattern is seen in the D_{50} profiles where a sudden strong increase of the values occurs between 25 and 30-m depth in the shear layer in the lower boundary layer between the bottom of the interflow and the ambient waters. It reaches values >20 μm from ∼30 to 45-m depth, mainly because of the strong contribution of macroflocs in this layer. From ∼45 m down to the bottom of the water column, D_{50} decreases again to ∼10 μm (Figure 6).

The corresponding 2-m averaged PSD at 5-m depth, at the interflow depth, and at 40-m depth provide further information on the in situ particle distribution in the interflow and in the surrounding waters (Figure 7). The PSD above the interflow at 5-m depth, is bimodal (except at station S2) with the first mode at 6.6 μm at all stations and the second between 183.5 and 216.17 μm (Figures 7a–7e). At this depth, the corresponding deflocculated PSD

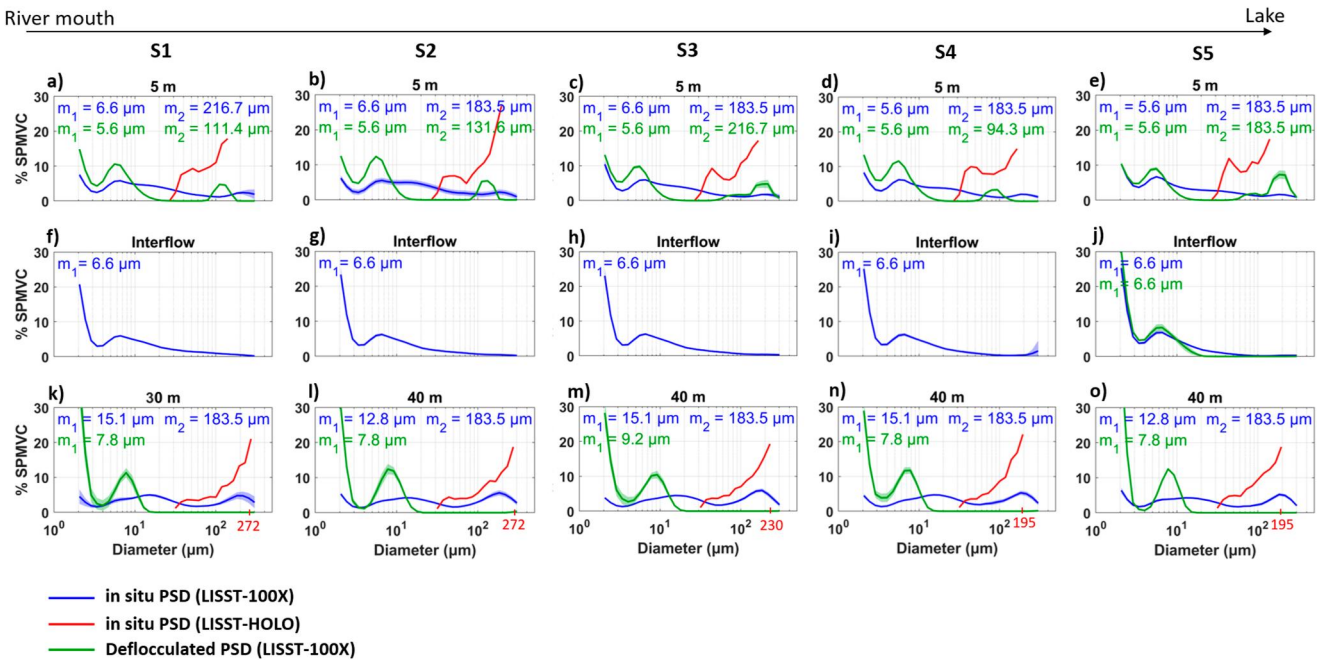

Figure 7. Particle size distribution (PSD; % of Suspended Particulate Matter Volume Concentration (SPMVC) for different size classes in µm) measured at stations S1–S5 at three depths: at 5 m, in the interflow and at 40 m. Blue lines: PSD (averaged over 2 m) derived from direct in situ measurements with the LISST-100X; green lines: PSD measured with the LISST-100X in the laboratory from the deflocculated water samples (2-min average). The particle size values corresponding to the modes are given in each panel. Red lines: PSD derived from direct in situ measurements with the LISST-HOLO (5-min average). Maximum LISST- HOLO sizes are indicated on the horizontal axis in red. Note that LISST-HOLO measurements are not available in the interflow.

obtained from water samples is bimodal with the first mode at 5.6 µm at all stations and the second oscillating between 111.4 and 215.7 µm, indicating that this second peak is not due to flocs. Modes are more pronounced in the deflocculated water samples. At the interflow depth (15 m depth for stations S1–S3 and 20 m depth for S4 and S5), the PSD is unimodal with a mode at 6.6 µm at all stations (Figures 7f–7j). This value is identical to that observed in the Rhône River (Figure 6). Below the interflow, at 40-m depth, the PSD all along the interflow pathway is bimodal with the first mode ~12.8–15.1 µm and the second at 183.5 µm (Figures 7k–7o), suggesting that fine particles with a mode at 6.6 µm in the interflow core do not strongly settle. The corresponding deflocculated PSD measured with the LISST-100X in the laboratory presents a unique mode at 7.8 µm at stations S1, S2, S4, and S5 and at 9.2 µm at S3 with no particles >20 µm. This suggests that the particles of mode ~12.8–15.1 µm were very small aggregates that could be disaggregated.

4.3.3. Particle Size Distribution and Shape From LISST-HOLO

At 5 and 40-m depths, the PSD derived from the in situ LISST-HOLO measurements reveals major contributions of particles >100 µm at each station, coinciding with small peaks in the LISST-100X observations (Figure 7). At 40-m depth, the size of the largest particles class observed by the LISST-HOLO decreased along the interflow pathway from 272 µm at S2 to 195 µm at S5. Due to the LISST-HOLO detection limit (see Section 3), neither PSD <30 µm, nor measurements within the interflow core can be obtained.

The above results and the POM content (<1.5%, Table S1 in Supporting Information S1) suggest that particles >20 µm observed below the interflow, at 40-m depth, by the two LISST instruments were flocculated inorganic particles, since they could be fully deflocculated into finer particles (clays and fine silts) (Figure 7). On the other hand, above the interflow at 5-m depth, the presence of large particles (>100 µm) in the deflocculated spectra and the POM content (~5%–9%, Table S1 in Supporting Information S1) suggest that the SPM also contained organic particles.

Representative samples of LISST-HOLO images at 5-m and 40-m depth at S2 allow characterizing the composition of the particle assemblage at these depths (Figure 8). In the near surface waters at 5-m depth, a large number of various planktonic organisms ~100 µm appear (Figure 8a), whereas particulate matter in the waters

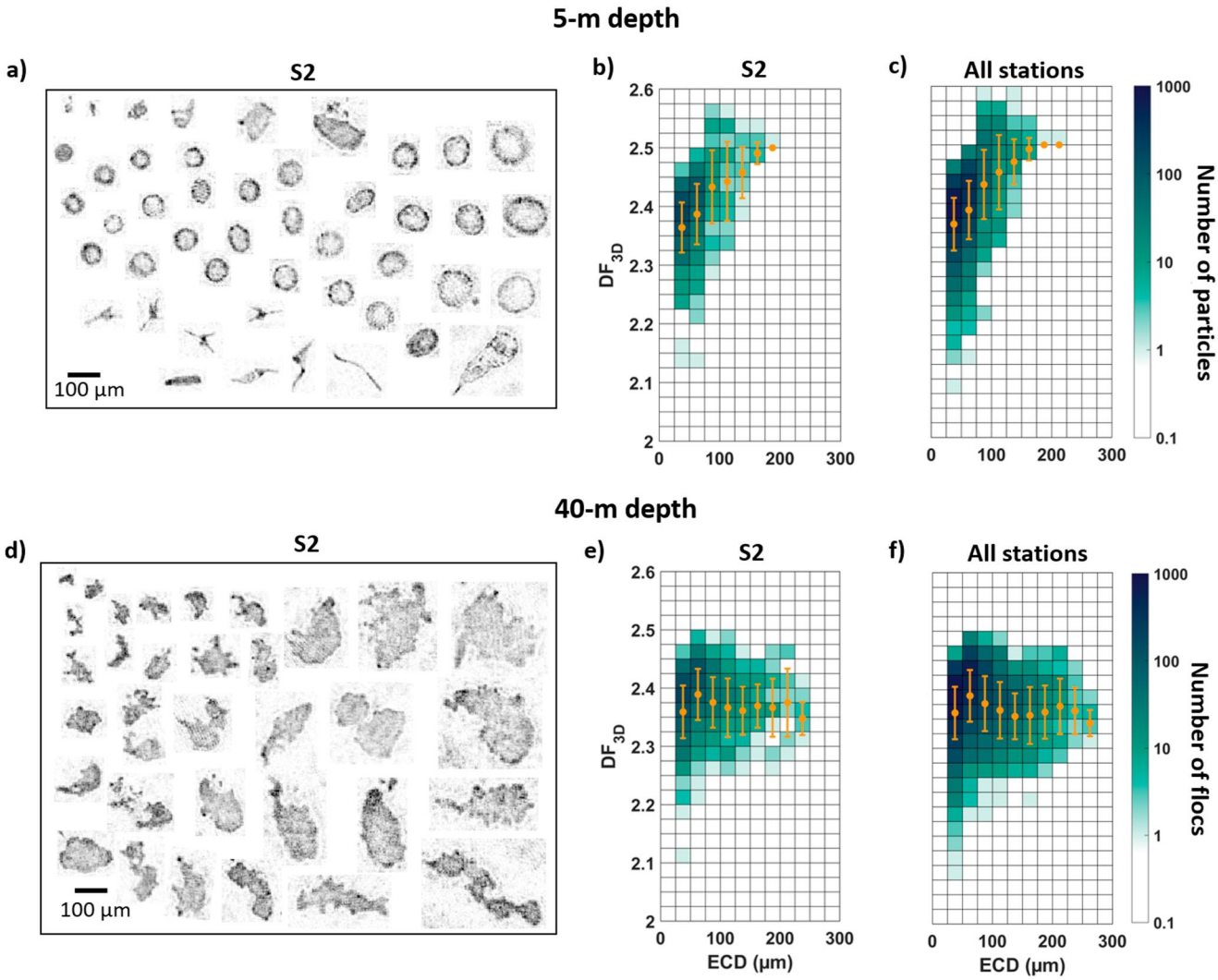

Figure 8. Representative examples of particle assemblage from the LISST-HOLO images at station S2 at: (a) 5-m and (d) 40-m depth. Density plots of the 3D fractal dimension of particles (DF_{3D}) as a function of the Equivalent Circular Diameter (ECD, µm) at station S2 at: (b) 5-m and (e) 40-m depth, and combined for all five stations at: (c) 5-m and (f) 40-m depth. The orange dots and error bars denote the mean DF_{3D} value per size class and the corresponding standard deviation.

below the interflow at 40-m depth is mostly composed of large flocs >100 µm (Figure 8d). A clear difference in structure can be seen between the samples of the two layers. In the near surface layer, flocs are mainly spherical and solid. Below the interflow at 40 m, macroflocs are spherical to elongated, loose to very loose, heterogeneous in composition and have a wide, skewed, plurimodal size distribution.

The corresponding qualitative and quantitative distribution of the three-dimensional (3D) fractal dimension of particles (DF_{3D}) (Equation S2 in Supporting Information S1) highlights a large diversity of particle shapes for the same size class, resulting in different fractal dimensions in the two layers (Figures 8b, 8c, 8e, and 8f; Figure S4 in Supporting Information S1). At 40-m depth, flocs of mineral composition >100 µm have DF_{3D} values ranging from 2.2 to 2.5 (Figures 8e and 8f; Figure S4 in Supporting Information S1). In contrast, the planktonic organisms >100 µm near the surface (5-m depth) have DF_{3D} values between 2.2 and 2.6 (Figures 8b and 8c; Figure S4 in Supporting Information S1). This shows that the shapes of the flocs at 40-m depth are more irregular (lower DF_{3D}) than the shapes of the organic particles at 5-m depth. The mean values indicate that the most abundant flocs at 40-m depth have a fractal dimension in the narrow range from ∼2.35 to 2.4 (Figure 8f; Figure S4 in Supporting Information S1), whereas the mean fractal dimension noticeably increases from ∼2.35 to 2.5 for the most abundant organic particles near the surface at 5-m depth (Figure 8c). This suggests that the largest organic particles are less fractal than the smallest ones. The non-mineral composition of the planktonic organisms

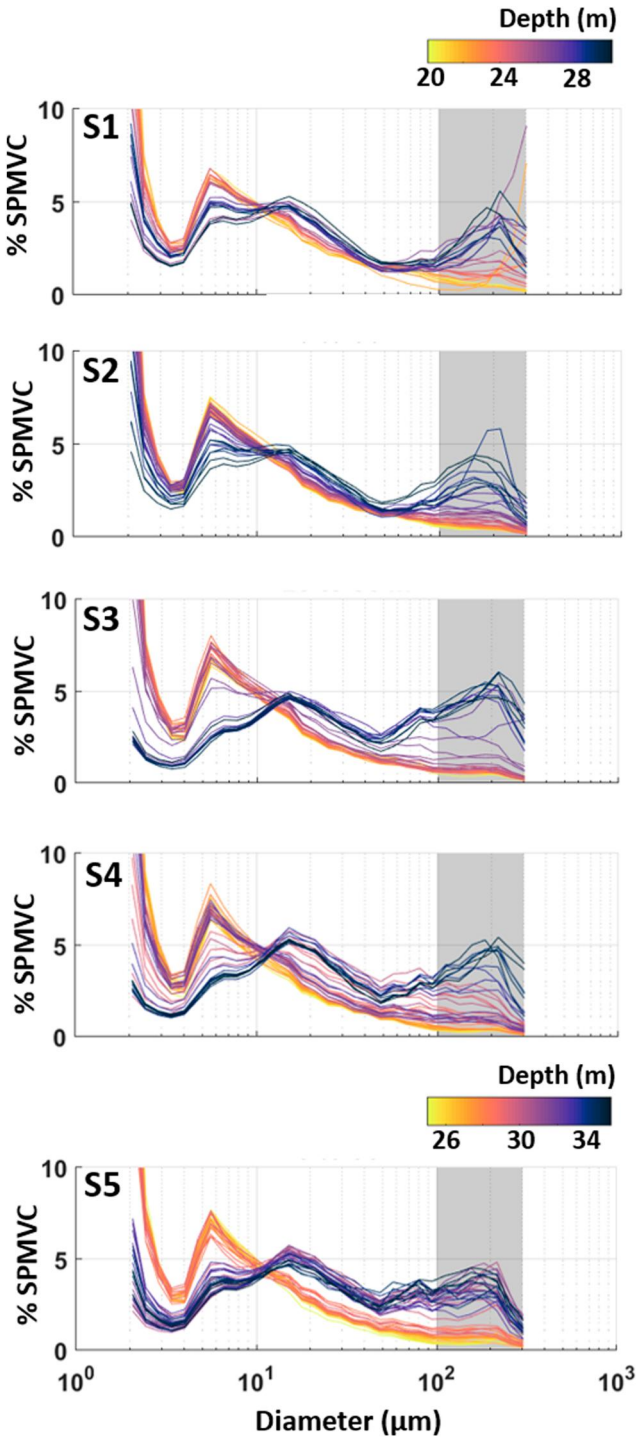

Figure 9. Particle size distribution (PSD; % of Suspended Particulate Matter Volume Concentration, SPMVC, for size classes in µm) from the LISST-100X measurements for 0.3-m thick layers between 20 and 30-m depth for stations S1–S4 and between 25 and 35-m depth for S5. The colorbars give the depth range. The macrofloc size range is shaded in gray.

explains the presence of particles >100 µm in the corresponding deflocculated PSD spectra at 5-m depth (Figure 7, top panels).

4.3.4. Particle Size Distribution From LISST-100X

The PSD spectra measured in ~0.3-m thick layers along the profile by the LISST-100X are detailed for the depth range of the shear layer between the bottom of the interflow and the water below as defined by the profiles of conductivity and SPM_{OPT} (Figure 3), RMS(v'), Γ, and λ_k (Figure 4) and D_{50} (Figure 6). The shear layer is located between 20 and 30-m depth for stations S1, S2, S3, S4 and between 25 and 35-m depth for S5 (Figure 9). With increasing depth, the PSDs change from unimodal (within the interflow, $\lesssim$ 25 m depth) to bimodal (in the shear layer, $\gtrsim$ 25 m depth). The dominant peak of clays and very fine silts (<8 µm) in the interflow layers rapidly disappears below ~25-depth with increasing distance from the river mouth. At the same time, the contributions of fine silts (8–20 µm), microflocs (20–125 µm) and in particular, macroflocs (>125 µm) progressively increase (Figures 6 and 9). The difference between the PSD in the interflow core and the shear layer is obvious at all stations. A two-layer structure is evident at the furthest station, S5.

In the shear layer between the bottom of the interflow and the surrounding water below, that is, between 20 and 30-m depth, a significant progressive transition occurs from the dominance of particles in the smaller size classes in the interflow above the shear layer to those in larger size classes in the shear layer. This is a clear indication that flocculation takes place in this shear layer, and large macroflocs form that are composed of the small particles observed in the interflow above. These macroflocs settle out of the shear layer and can be visualized at 40 m depth in the hypolimnion below (Figure 8).

5. Discussion

Hydrodynamics of interflow formation, plume spreading and entrainment in the nearfield of the Rhône River inflow have been previously studied in detail (Piton et al., 2022; Soulignac et al., 2021). It was found that when lake current velocities are small, the inflow plume of the negatively-buoyant Rhône River flows straight out from the river channel, plunges rapidly as is evident in the triangular plume shape on the surface (Figure 1c) and then forms an interflow in the thermocline within a short distance from the mouth. It was also demonstrated that the interflow plume mainly spread laterally, unconfined with distance from the mouth due to entrainment, but remained vertically confined in a thin layer in the thermocline. A core zone was established in the interflow plume where normal horizontal velocities changed little along the pathway. The core zone progressively reduced in size with distance from the mouth due to lateral entrainment. A bimodal PSD was observed in the interflow at all stations and PSD evolution along the pathway reflected the change in core zone size. The same pattern of these principal interflow features was also seen in the field data of the present study (Figures 3 and 4; Figure S1 in Supporting Information S1), thus indicating that the present study is representative for Rhône River interflow dynamics.

Below, the flocculation dynamics in relation to this interflow plume development are considered, in particular, the changes of PSD in the vertical and their relationship to hydrodynamic parameters.

5.1. In Situ Characterization of Flocs

Our analysis of the sediments brought into the lake by the Rhône River indicates that they are a mixture of clay and fine silts (Figure 5). Clays are cohesive, whereas silts are mostly non-cohesive. As pointed out by Tran and Strom (2017), it was long not clear whether silts could be integrated into clay flocs. An experimental investigation conducted by Tran and Strom (2017) on the settling behavior of clay and silt mixtures indicated that silt particles, independent of their size, could become bound within clay flocs and that the silt content had no significant effect on floc size. However, the trapping of silt particles within flocs can have an important impact on floc density, and thus on the settling velocity which may increase by more than 50% (Tran & Strom, 2017; Xu et al., 2022). These results were confirmed by river studies (Osborn et al., 2023) and agree with Droppo and Ongley (1994), indicating that salinity is not a needed for sediments to flocculate. Therefore, it can be assumed that the flocs generated in the Rhône River interflow shear layer are a mixture of clays and silts.

LISST-100X measurements taken along the interflow pathway in 2018 (Piton et al., 2022) showed a contribution of large particles >63 µm. At that time, their shape and composition could not be determined in that study. Therefore, it was suggested that the largest particles are fine sands brought in by the Rhône River inflow, in accordance with Burrus et al. (1989) who interpreted the presence of large particles >63 µm in the Rhône River as fine sands, based on turbidity measurements. However, in the present study, it could be determined that no fine sands were found in the water samples from the Rhône River (Figure 5). The holographic measurements clearly revealed for the first time that the largest particles detected below the interflow (>100 µm; ∼30 to 45-m depth) are actually inorganic micro- and macroflocs generated from small clay and silt particles carried by the Rhône River interflow (Figures 5–7). In the near-surface waters, large particles are predominantly phytoplanktonic organisms (Figure 8). These are not brought into the lake by the Rhône River inflow, since its Particulate Organic Matter content (POM) of the total SPM is below 1.5%, whereas the POM content in the lake is ∼5%–9% at 5-m depth.

The floc size in the hypolimnion below the Rhône interflow pathway ranges from ∼20 to 280 µm (Figure 8), which is comparable to the typical floc size range observed in the Lillooet Lake hypolimnion (Hodder & Gilbert, 2007). Water samples showed that the organic matter content in the SPM assemblage was low (<1.6%, Table S1 in Supporting Information S1), which is consistent with the absence of floc-associated organic material reported in glacier-fed rivers (Woodward et al., 2002). Even though it has been established that the LISST can correctly resolve particle size distributions, it was observed that estimates of large size particle concentration may be affected by schlieren when density gradients are present, such as in the lower layers of the interflow. Schlieren, the scattering by density fluctuations, occurs in microscale turbulent shear which scales with the Kolmogorov scale. Kolmogorov scales (∼200–300 µm) were observed in the shear layers in the lower boundaries of the interflow (Figure 4). Styles (2006) had determined that schlieren may concern particles >128 µm. Mikkelsen et al. (2008) have identified schlieren as contributing to an increase in particle volume for buoyancy frequencies N ranging from 0.02 to 0.05 s^{-1}. The buoyancy frequency in the shear layer at the bottom of the interflow was $N \approx 0.015$ s^{-1} at all stations. Thus, our LISST measurements were not affected by schlieren.

The observed sizes are smaller than the typical floc size range of 30–600 µm observed in the Ems, Rhine, Gironde, Tamar and Po estuaries where salinity may contribute to the floc formation (Eisma, 1991; Fennessy et al., 1994; Fox et al., 2004; van Leussen and Cornelisse, 1994), and also smaller than the typical floc size of 20–500 µm in coastal marine waters where again salinity plays a role (Many et al., 2019; Mikkelsen & Pejrup, 2001), and in lowland riverine waters (Thonon et al., 2005). In addition, the differences in size may be explained by the observed low organic matter content, and thus EPS, that is recognized to be an important component of flocs in estuarine, lowland rivers and marine waters (Deng et al., 2022; Droppo et al., 1997; Mari et al., 2011; McConnachie & Petticrew, 2006).

The time to equilibrium depends on the type of sediment and water, turbulence level and size distribution of the initial suspension. Laboratory studies suggest that lake sediment macroflocs reach equilibrium size in 50 min to 1 hr (Chakraborti et al., 2007; Tsai et al., 1987). Winterwerp (1998) indicated that flocs may never reach equilibrium size, if the time flocs are suspended in the turbulent water column is less than the flocculation time. However, results of laboratory studies should be interpreted with caution, since they are most often carried out under idealized conditions and do not take into consideration the complex interaction of different hydrodynamic and sedimentary processes that contribute to flocculation; these equilibrium time values cannot be verified in field studies.

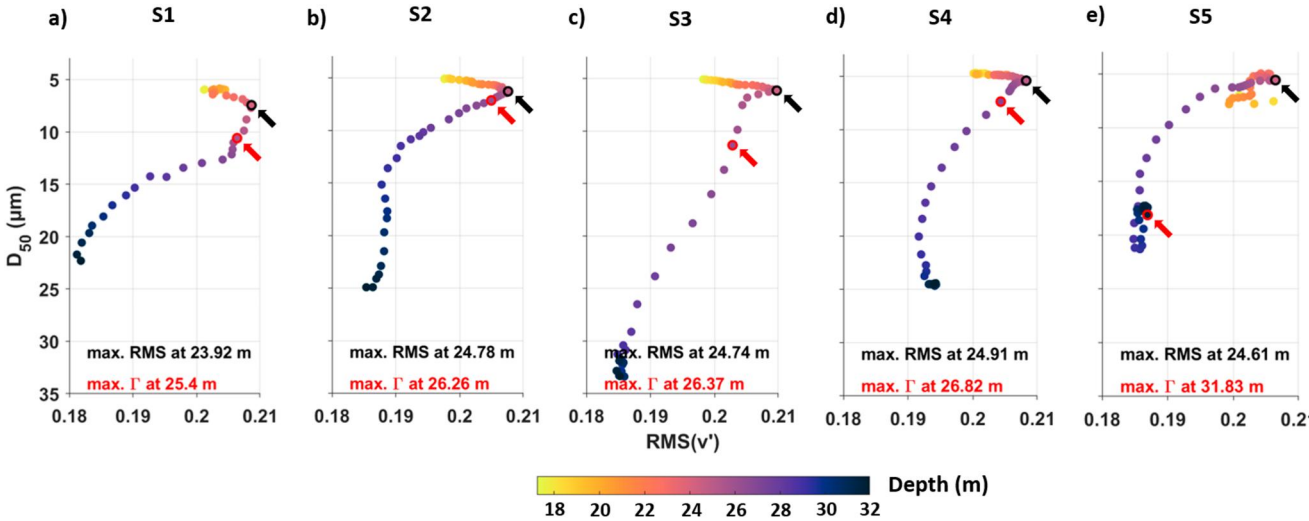

Figure 10. Relationship between D_{50} and RMS(v') in the depth range from 17 to 32-m at stations S1 to S5. The depths at which the maxima of RMS(v') and of (Γ) are reached is marked by the black and red arrows, respectively; compare to Figure 4. The color coding of the points corresponds to depth values as indicated in the legend.

On the other hand, it has been shown that maximum floc size is proportional to the Kolmogorov microscale (van Leussen, 1997; Verney et al., 2009; Winterwerp et al., 2006). This concept can be verified by measurements in field studies. In the Rhône River interflow, equilibrium between the forcing and the floc size was already observed at station S2, located 400 m from the river mouth, where the maximum size of the flocs corresponds to the Kolmogorov scale (Figures 4 and 7). Assuming that interflow was established at ∼200 m from the mouth, after river plunging (Figure 1c) and underflow (Figure 2), and a mean interflow flow speed of ∼15 cm s^{-1} (Figure 4), flocs can reach equilibrium floc size within O(30 min). This is much shorter that the equilibrium time reported in laboratory studies, thus suggesting that idealized laboratory studies may produce equilibrium time scales that are not representative for those observed in the field.

Floc shapes are controlled by various mechanisms that interact with each other such as turbulence, sediment concentration, differential settling, organic content and biogenic aggregation (Manning & Dyer, 2002; McCave, 1975; Verney et al., 2009; Winterwerp, 1998). In the present study, the floc perimeter-based three-dimensional (3D) fractal dimension, DF_{3D}, is used to characterize floc shape. The range of DF_{3D}, ∼2.1–2.5 (Figures 8c and 8f), is similar to previous plume studies in the Rhône River plume in the Mediterranean Sea (DF_{3D} ∼ 2.0–2.5; Many et al., 2019), in Glacier Bay (DF_{3D} ∼ 2.4; Hill et al., 1998) and in the Tamar Estuary (DF_{3D} ∼ 2.0–2.5; Maggi et al., 2006). The present estimates are also comparable with the fractal dimensions of aggregates of latex beads (DF_{3D} ∼ 2.25 ± 0.11) generated by turbulence and shear in the laboratory (Thill et al., 1998), and with the fractal dimensions of the mud flocs compiled in Strom and Keyvani (2011). Overall, these estimates fall in between those fractal dimensions of aggregates similar to marine snow formed by Brownian motion in diffusion-limited cluster aggregation (DF_{3D} ∼ 2.09 ± 0.11; Thill et al., 1998), and of aggregates similar to sludge flocs formed in reaction-limited cluster aggregation (DF_{3D} ∼ 2.4 ± 0.12; Thill et al., 1998). For the observed range of floc perimeter-based fractal dimensions (DF_{3D} ∼ 2.1–2.5) in the Rhône River interflow, turbulence and shear therefore are important in their formation.

5.2. Effects of Turbulence

The effect of turbulent structures on floc size is examined in the shear layer between the bottom of the core of the interflow (∼20-m depth) and the water below (∼30-m depth) (Figure 10). This layer was identified as the layer in which flocculation is initiated (Figure 9), and where a significant increase of D_{50} is observed (Figures 4 and 6). The maximum of the RMS(v') parameter, ∼0.205–0.21, is found between 24 and 25-m depth (Figures 4 and 10), and the maximum shear stress (Γ) is reached at ∼26-m depth, with values ranging from 15 to 27 s^{-1} for stations S1–S4 (Figures 4 and 10). Above the depth of maximum RMS(v') (in the interflow), D_{50} values are small (∼5–7 µm) (Figure 10). Below that depth (in the shear layer), D_{50} increases rapidly to values ∼20–34 µm at ∼30-m

Table 1
Values of Kolmogorov Microscale λ_k, Equivalent Circular Diameter, and the Longest Major Axis of Flocs Ax_{maj} Found in Particle Assemblages Measured by the LISST-HOLO, for Stations S1 to S5 at 40-m Depth

Station	S1	S2	S3	S4	S5
Distance from river mouth (m)	350	400	800	1,200	1,500
λ_k (μm)	281	394	337	290	202
ECD (μm)	272	272	230	195	195
Ax_{maj} (μm)	295	401	333	286	208

depth (Figures 6 and 10). This indicates the important effect of turbulence on floc formation and agrees with the fractal analysis (DF_{3D}).

It appears that the level of turbulent fluctuations of the normal velocity component (>0.205) and of shear stress (>15 s^{-1}) in the ~25 to 32-m depth shear layer are sufficiently large to limit the gravitational settling of particles and to maintain them in suspension for a sufficiently long period in the shear layer to allow particle collisions and flocculation and to form flocs whose size is determined by the Kolmogorov microscale. This finding agrees with Dyer (1989) who showed from laboratory experiments that for comparable SPM concentrations (~50 mg l^{-1} at 25-m depth; Figure 3), floc sizes progressively increase under increasing shear stress conditions up to ~0.5 dyn cm^{-2} (corresponding to ~40 s^{-1}, taking the dynamic viscosity of water at 10°C). When shear stress further increased in his experiments, from 0.5 to 8 dyn cm^{-2} (~40–~600 s^{-1}), floc sizes rapidly decreased due to floc breakup. This agrees with Biggs and Lant (2000) who found in their experiments that large sludge flocs (median diameter ~120 μm) formed at a shear stress of 19.4 s^{-1}, whereas their sizes decreased to ~20 μm at a high shear stress of 343 s^{-1}.

At 40-m depth, the maximum floc diameter (ECD) and the maximum length of the longest axis (Ax_{maj}) decreased with distance from the river mouth (Figure 8; Table 1). Both the values of ECD and Ax_{maj} and their decrease correlated well with the Kolmogorov microscale (λ_k), which decreased from 394 μm at stations S2 to 202 μm at S5, at 40-m depth (Figure 4; Table 1). This confirms that the Kolmogorov microscale has the strongest positive correlation with floc size, supporting the concept that turbulent shear limits floc size. The maximum floc size along the Rhône interflow pathway is controlled by the smallest turbulent eddies as was observed in laboratory, estuarine and marine studies (van Leussen, 1997; Verney et al., 2009; Winterwerp et al., 2006) and contrasts with the lowland river environment where organic matter content is higher and flocs are ~2 times greater than the Kolmogorov microscale (Izquierdo-Ayala et al., 2021).

In the interflow, the Kolmogorov microscale λ_k ranges between 450 and 350 μm along the interflow pathway (Figure 4). However, in this layer, the levels of turbulent fluctuations and shear stress are low (<0.2 and <10 s^{-1}, respectively; Figure 4). It is hypothesized that these levels are too low to generate residence times long enough for large particle aggregation, and that they might favor particle settling. In addition, Izquierdo-Ayala et al. (2021) showed that shear stress <5 s^{-1} was not sufficient to generate macroflocs, and corresponds to the range given by Dyer (1989). Mikeš and Manning (2010) suggest that a Kolmogorov microscale λ_k of 240 μm indicates highly turbulent conditions, and turbulence levels are lower for larger λ_k, as confirmed in the present study.

A rapid change from small clay/silt particles in the interflow core to large macroflocs in the shear layer over a vertical distance of only a few meters is observed (Figure 9). Since the shear layer is documented all along the nearfield from stations S1 to S5, and macroflocs are found below the shear layer at all stations along the nearfield trajectory, it can be assumed that macrofloc formation occurs all along the nearfield of the interflow plume. Even though the shear layer is relatively thin, our findings show that it is a crucial layer in the nearfield dynamics with respect to flocculation. Our water column measurements were made at stations in the center of each transect. However, from transect measurements (Figure S1 in Supporting Information S1; Piton et al., 2022), it can be seen that the interflow core has a certain lateral extension. It can be expected that a shear layer exists over a certain width below the interflow, thus suggesting that macrofloc formation and subsequent settling can occur over this width.

5.3. Effects of SPM Concentration

In the present study, flocculation leads to large macrofloc formation in the shear layer located between the bottom of the interflow and the water below at 20 to 30-m depth (Figures 6, 7, and 9). From 20 to 30-m depth, SPM_{OPT} concentrations decrease from 50 to 80 to <2 mg l^{-1} at all stations (Figure 2). Previous laboratory experiments showed that fine-grained lake sediment flocculation occurred at concentrations of 50–100 mg l^{-1} (for a constant shear stress of 2 dyn cm^{-2}, ~150 s^{-1}), generating flocs of ~80–120 μm (Lick & Lick, 1988). The rather high SPM concentrations at the bottom of the interflow combined with turbulent mixing, therefore, could favor collisions and the formation of large flocs.

In the interflow, SPM_{OPT} concentrations range between 50 and 100 mg l^{-1}, with values decreasing with distance from the river mouth (Figure 3). This decrease in SPM_{OPT} along the interflow pathway may be attributed to both the settling of particles and the dilution of the Rhône interflow with ambient lake waters (Piton et al., 2022). These concentrations, however, should not limit flocculation (Lick & Lick, 1988; Mikeš et al., 2004). It is therefore suggested that the low turbulence levels discussed above, limit floc growth in the interflow ($\lesssim$10 µm; Figures 6 and 8).

At 40-m depth, where macroflocs up to ~300 µm are observed (Figure 8), SPM_{OPT} is <2 mg l^{-1} (Figure 3). These results are similar to the observations reported for Lillooet Lake (Hodder & Gilbert, 2007). From the present measurements, it is not possible to determine whether flocs can still form at this depth, or whether their presence is due to differential settling from the layers above (McCave, 1975). Although differential settling is negligible in a high-energy environment (rivers, estuaries), it may become important in low energy layers such as the hypolimnion in lakes. Lick et al. (1993) have shown that the time to steady state and steady state floc diameters are larger when differential settling is the dominant mechanism for flocculation rather than fluid shear. Settling velocities of the flocculated particles were larger and increased more rapidly with floc diameter when produced by differential settling than when fluid shear is dominant. The observed low SPM concentrations might not limit flocculation since previous studies reported that flocculation is still significant for concentrations <10 mg l^{-1} in the Seine estuary (Verney et al., 2009) and in the Rhône River plume (Many et al., 2016). However, shear and turbulence are low in the present study (Figure 4). In addition, the POM contents of the total SPM remain very low at this depth (<1.6%), and therefore cannot significantly contribute to macrofloc formation.

5.4. Implications for Sediment Fluxes

Previous studies reported floc settling velocities of 1–5 mm s^{-1} (e.g., Fennessy et al., 1997; Hawley, 1982). These exceed those of their constituent grains (Stokes settling velocity) of 0.07 mm s^{-1} for 10 µm sized particles by an order of magnitude. Furthermore, floc shapes should be considered when estimating settling velocities (Many et al., 2019). In the absence of measured settling velocity or floc density estimates, the settling velocity formulation of Strom and Keyvani (2011; Equation 18) may be used as a first-pass estimate of the floc settling velocity based on measured floc sizes:

$$W_s = \frac{gR_s}{b_1 v d_p^{nf-3}} d_f^{nf-1}$$

with g the acceleration of gravity (9.81×10^3 mm s^{-2}), R_s the submerged specific gravity of the primary particles ($R_s = (\rho_s - \rho)/\rho = (2{,}630 - 1{,}000)/1{,}000 = 1.63$), b_1 the particle shape coefficient (here equals to 20), v the horizontal velocity of the flow in the hypolimnion (50 mm s^{-1}), d_p the diameter of the primary particles (6.6 µm), d_f the diameter of the flocs (200 µm), and nf the fractal dimension. If primary particles are considered to be spherical (Strom & Keyvani, 2011), $nf = 3$, and we obtain a settling velocity value of 1.82 mm s^{-1}, which does not differ much from the estimates of Manning and Dyer (2002) and those reported for clay/silt flocs by Nghiem et al. (2022). The surface heterogeneity of the particles may make them less spherical. This may be the case in the Rhône River since the river is short and the sediment is mainly produced by the break-up of rocks along its path. Heterogeneous surfaces, however, increase the attachment of particles (Cui et al., 2023).

Based on the above, if we consider particles to be less spherical ($nf = 2.9$), we obtain $w_s = 1.1$ mm s^{-1}; with $nf = 2.8$, $w_s = 0.66$ mm s^{-1}. Livsey et al. (2022) observed settling velocities of O (1 mm s^{-1}) once silts and clays have flocculated; this value is also suggested by Strom and Keyvani (2016) as a first approximation.

The above settling velocity values can only be considered as rough estimates, since certain aspects, such as porosity have not been taken into consideration. Porosity determines the degree to which water can flow through floc pores and thus influence drag and settling rates of suspended material (Strom & Keyvani, 2016). Porosity increases with floc size and largest porosity is found in the largest macroflocs (Droppo et al., 2000). The results of Droppo et al. (2000) demonstrated that as floc size increases, the settling velocity increases. Wheatland et al. (2020) reported that some of the smaller porosities may be filled with EPS and this may affect the flow of water through the pores and thus the settling velocity (Strom & Keyvani, 2016). In our case, however, this may only be a process of secondary importance, since POM is low.

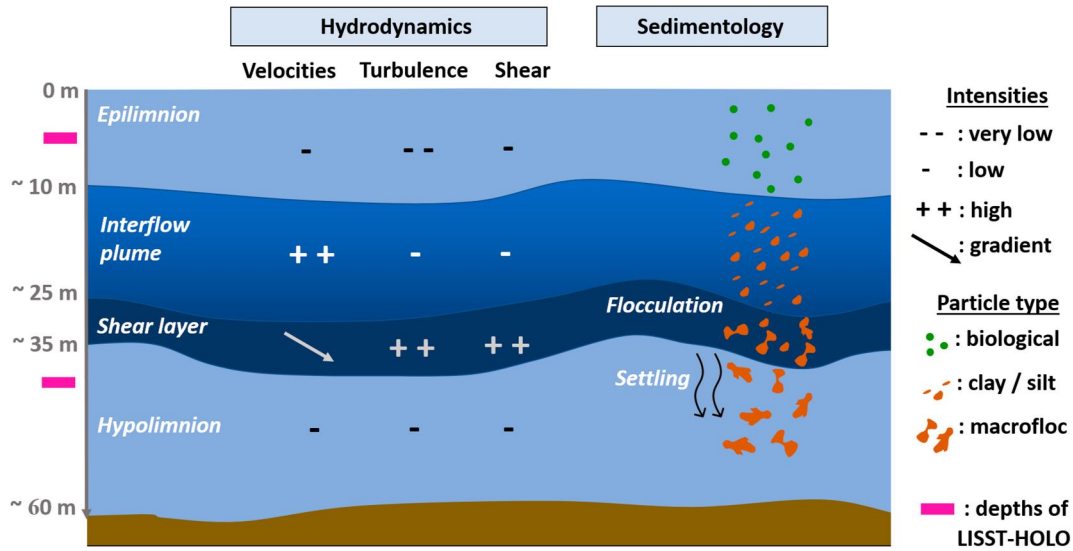

Figure 11. Schematic representation of processes leading to macrofloc formation in the shear layer between the bottom of the Rhône River interflow plume and the hypolimnion below. Note that flocculation and macrofloc formation only occur in the shear layer. See Figure 3 for the formation of the interflow plume layer.

Using the above estimates, the distance traveled by the flocs while settling out, can be estimated. The flocs could settle ~30 m (from the shear layer to the bed) in ~4–12 hr. While settling, the flocs may then be transported by currents over a horizontal distance of ~750 m to 2.25 km. As a result, settling flocs will reach the lakebed while they are still in the interflow nearfield area. The above estimates, assuming that macroflocs strongly contribute to the settling of SPM, could support the findings of Loizeau et al. (2012) and Silva et al. (2019), who observed that sedimentation rates in the Rhône River delta are inversely proportional to distance from the river mouth, with rates near the mouth ranging from ~0.05 m y^{-1} to as high as 0.4 m y^{-1}. These rates are much higher than those measured further away from the nearfield (O(1 mm y^{-1})) and could not result from Stokes settling of the small clay and silt particles brought in as suspended load by the Rhône River and observed in the interflow.

Fine sediments assembled into flocs can therefore create pollutant hotspots in the nearfield. However, if they do not flocculate, primary sediment particles may travel in suspension over long distances instead (Ishiguro & Balvay, 2003). In Lillooet Lake, the sediment flux attributed to macroflocs was equivalent to one-quarter of the average annual sediment flux (Hodder, 2009). The settling of SPM out of the interflow by flocs could explain the decreasing sediment flux along the nearfield interflow pathway reported by Piton et al. (2022).

Future field studies should investigate flocculation dynamics during the low discharge season, since the energetic environment, organic content and sediment discharge may differ. In addition, such studies should include estimations of sediment fluxes occurring along the Rhône interflow pathway due to macroflocs settling via direct in situ measurement of settling velocities. It has been pointed out that laboratory studies of flocculation and floc settling can only be rough approximations of reality, since they cannot take into consideration the complex interplay of the different hydrodynamic, sedimentary and biological processes that contribute to flocculation dynamics in the field.

5.5. Significance of the Findings

This study addressed for the first time, flocculation in a river plume interflow in a lake. The interflow flow field is very different from that in rivers, estuaries and oceans as reported in the literature. An interflow resembles a plane jet in a quiescent ambient and is a layer in which velocities are significantly higher than in the surrounding ambient (Figures 3–5). This leads to the generation of shear layers between the interflow and the ambient. In particular, the presence of the shear layer at the bottom of the interflow is, therefore, crucial for triggering flocculation in the nearfield of the river plume interflow (Figure 11), because hydrodynamic and sedimentary conditions in this layer are favorable to flocculation initiation, and are of the same order as in other flow fields (rivers, estuaries, oceans). Flocculation was only observed in the shear layer (Figure 9), which is relatively thin

compared to the total water depth. This is different from the situation in river and estuarine flows where flocculation occurs over most of the water column.

Different from river and estuary flows, the interflow field is not in contact with the bed (Figures 2, 3, and 11) and thus a sediment exchange between the bed and the flow which can replenish the suspended sediment charge in rivers and estuaries, cannot happen in an interflow. Therefore, with distance from the mouth, the initial sediment quantity carried by the Rhône River will not only diminish due to floc generation and settling of flocs, but also due to dilution of the interflow plume caused by unconfined spreading and entrainment. Since we visualized macroflocs in the hypolimnion below the shear layer along the whole length of the nearfield, settling velocities appear to be high enough to allow settling of most of the macroflocs in the nearfield area which increases the risk of hot spot formation. We have previously shown (Soulignac et al., 2021) that the Rhône River interflow plume may meander and as a result, extend the surface of the hot spot. This is again different from rivers and estuaries where the sediment is continuously resuspended and spread over long reaches, but guided by the river channel.

6. Summary and Conclusions

The results of this field study, carried out in Lake Geneva, provided unique insight into suspended particle property dynamics along the nearfield of a river interflow plume in a lake. Detailed simultaneous measurements of turbulence combined with profiles of temperature, conductivity, turbidity and PSD and water samples allowed determining the factors that enhance or limit suspended sediment flocculation along the water column. For the first time in a lake, holographic camera images captured floc formation below a river interflow plume and allowed the characterization of floc composition, size and shape above and below the interflow.

The analysis showed that:

- During the stratified period, the Rhône River plume flowed as an unconfined interflow within the metalimnion located between ∼10 and 30-m depth, with normal velocities (v) up to ∼0.25 m s^{-1} in the core of the interflow (Figure 11). The core normal velocities decreased along the pathway to ∼0.1 m s^{-1} at 1,700 m from the river mouth mainly due to lateral entrainment of ambient waters. These measurements confirmed previous unconfined Rhône River plume spreading observations.
- Shear layers are formed between the high velocity interflow core and the low velocity ambient (Figure 11). High levels of shear (Γ = 15 to 27 s^{-1}) in the upper and lower shear layers, measured for the first time in the field, indicated strong mixing due to shear. Turbulence fluctuation levels, RMS(v'), were highest in the shear layer.
- The SPM composition varied along the water column. Three distinct layers were identified: (a) Above the interflow in the near surface waters, SPM was composed of phytoplanktonic organisms (up to ∼200 μm) which is characteristic for the lake background, microflocs (∼20–100 μm), and clays and silts (<20 μm), (b) In the interflow core, where the sediment load was the highest, SPM composition was similar to that of the Rhône River, and mainly composed of clays, silts and some microflocs, and (c) In the hypolimnion below the interflow, where the sediment load was the lowest, most of the SPM volume consisted of macroflocs (∼100–300 μm) and microflocs, with small amounts of fine grains (<20 μm) (Figure 11).
- All along the interflow pathway, the largest flocs (macroflocs) were formed in the bottom shear layer (Figure 11). Sufficiently high levels of turbulent fluctuations of the normal velocity component and of shear stress combined with sufficiently high SSC persisted in the shear layer and were identified as the main parameters enhancing macrofloc formation. Our study revealed that the existence of this shear layer is crucial for macrofloc formation in the Rhône River nearfield.
- Levels of turbulence and Γ values were low within the interflow core which limited macrofloc growth in the interflow core, despite high SPM concentrations.
- Macroflocs settled out from the bottom shear layer, since their settling velocity is expected to be much higher than that of the disaggregated fine particles. Fine particles remained in suspension in the interflow core and were transported further out into the lake, allowing macrofloc formation in the bottom shear layer all along the interflow plume pathway in the nearfield.
- The smallest turbulent eddies measured by the Kolmogorov microscale controlled the maximum macroflocs size at 40-m depth, consistent with marine and estuarine observations.

- The range of the floc fractal dimensions ($DF_{3D} \sim 2.1–2.5$) observed below the shear layer indicates that flocs that formed along the Rhône River interflow pathway have an intermediate shape complexity between marine snow and sludge flocs, and that turbulent shear is important in their formation.
- Salinity is not needed for floc formation in Lake Geneva.

By investigating and characterizing SPM, in particular, the formation and evolution of flocs along a negatively-buoyant inflow into a large lake (Lake Geneva), this study has contributed to better understanding the dynamics of suspended sediments and their fate in lacustrine systems; it was demonstrated that results from marine systems and estuaries cannot be directly applied in lakes. Such knowledge, which is presently lacking, can help determine how nutrients and contaminants attached to sediment particles brought into the lake by rivers, will spread or be deposited. The effects of flocculation on the transport and dispersion of suspended particles and on sediment flux should therefore be taken into consideration when developing effective lake management concepts for Lake Geneva. Since the analysis was based on universally valid concepts, the results can also be expected to be valid for river plume interflows in other lakes under comparable conditions.

Conflict of Interest

The authors declare no conflicts of interest relevant to this study.

Data Availability Statement

The CTD, LISST-100X and Signature1000 data are archived on Zenodo (Piton et al., 2023a). The Holo-batch software is available upon request at support@SequoiaSci.com (Sequoia Scientific, Inc., 2018). The LISST-HOLO images (.tiff) and corresponding post-processed files generated by the Holo-batch software are archived on Zenodo (Piton et al., 2023b).

Acknowledgments
The authors thank SAGRAVE (http://www.sagrave.ch/) for their assistance with logistics. The authors would also like to thank Dr. Gaël Many for meaningful discussions during the data treatment. The authors warmly thank the reviewers and the associate editor for their work during the revision process of this article. Open access funding provided by Ecole Polytechnique Federale de Lausanne.

References

Agrawal, Y. C., & Pottsmith, H. C. (2000). Instruments for particle size and settling velocity observations in sediment transport. *Marine Geology*, *168*(1–4), 89–114. https://doi.org/10.1016/s0025-3227(00)00044-x

Andrews, S., Nover, D., & Schladow, S. G. (2010). Using laser diffraction data to obtain accurate particle size distributions: The role of the particle composition. *Limnology and Oceanography: Methods*, *8*(10), 507–526. https://doi.org/10.4319/lom.2010.8.507

Biggs, C. A., & Lant, P. A. (2000). Activated sludge flocculation: On-line determination of floc size and the effect of shear. *Water Research*, *34*(9), 2542–2550. https://doi.org/10.1016/S0043-1354(99)00431-5

Bowers, D. G., McKee, D., Jago, C. F., & Nimmo-Smith, W. A. M. (2017). The area-to-mass ratio and fractal dimension of marine flocs. *Estuarine, Coastal and Shelf Science*, *189*, 224–234. https://doi.org/10.1016/j.ecss.2017.03.026

Burkard, P. (1984). Hydrologie – Bilan hydrologique. In *Commission Internationale pour la Protection des Eaux du Léman (CIPEL). Le Léman Synthèse 1957–1982* (pp. 43–48).

Burrus, D., Thomas, R. L., Dominik, J., & Vernet, J.-P. (1989). Recovery and concentration of suspended solids in the upper Rhône River by continuous flow centrifugation. *Hydrological Processes*, *3*(1), 65–67. https://doi.org/10.1002/hyp.3360030107

Chakraborti, R. (2005). Effects of floc size and shape in particle aggregation. In G. Droppo, G. G. Leppard, S. N. Liss, & T. G. Milligan (Eds.), *Flocculation in Natural and Engineered Environmental Systems*. CRC Press.

Chakraborti, R., Gardner, K. H., Kaur, J., & Atkinson, J. F. (2007). In situ analysis of flocs. *Journal of Water Supply: Research & Technology - Aqua*, *56*, 1–11. https://doi.org/10.2166/aqua.2007.063

CIPEL. (2019). Rapports sur les études et recherches entreprises dans le bassin lémanique, Campagne 2018. Nyon: Commission Internationale Pour la Protection des Eaux du Léman (CIPEL). Retrieved from https://www.cipel.org/wp-content/uploads/2019/10/RapportScientifique_camp_2018-1.pdf

Cui, Z., Huang, L., Fang, H., Bombardelli, F. A., Wang, D., & Wu, X. (2023). Attachment efficiency among fine sediment considering surface heterogeneity. *Journal of Hydraulic Research*, *61*(4), 452–469. https://doi.org/10.1080/00221686.2023.2222095

Curran, K. J., Hill, P. S., Milligan, T. G., Mikkelsen, O. A., Law, B. A., Durrieu de Madron, X., & Bourrin, F. (2007). Settling velocity, effective density, and mass composition of suspended sediment in a coastal bottom boundary layer, Gulf of Lions, France. *Continental Shelf Research*, *27*(10–11), 1408–1421. https://doi.org/10.1016/j.csr.2007.01.014

de Boer, D. H., Stone, M., & Levesque, L. M. J. (2000). Fractal dimensions of individual flocs and flocs population in streams. *Hydrological Processes*, *14*, 653–657. https://doi.org/10.1002/(SICI)1099-1085(200003)14:4<653::AID-HYP964>3.0.CO;2-3

Deng, Z., Huang, D., He, Q., & Chassagne, C. (2022). Review of the action of organic matter on mineral sediment flocculation. *Frontiers in Earth Science*, *10*, 965919. https://doi.org/10.3389/feart.2022.965919

Droppo, I. G., Jeffries, D., Jaskot, C., & Backus, S. (1998). The prevalence of freshwater flocculation in cold regions: A case study from the Mackenzie River delta, Northwest Territories, Canada. *Arctic*, *51*(2), 155–164. https://doi.org/10.14430/arctic1056

Droppo, I. G., Leppard, G. G., Flannigan, D. T., & Liss, S. N. (1997). The freshwater floc: A functional relationship of water and organics and inorganic floc constituents affecting suspended sediment properties. *Water, Air, and Soil Pollution*, *99*(1–4), 43–53. https://doi.org/10.1007/BF02406843

Droppo, I. G., & Ongley, E. D. (1992). The state of suspended sediment in the freshwater fluvial environment: A method of analysis. *Water Research*, *26*(1), 65–72. https://doi.org/10.1016/0043-1354(92)90112-H

Droppo, I. G., & Ongley, E. D. (1994). Flocculation of suspended sediment in rivers of southeastern Canada. *Water Research*, *28*(8), 1799–1809. https://doi.org/10.1016/0043-1354(94)90253-4

Droppo, I. G., Walling, D. E., & Ongley, E. D. (2000). The influence of floc size, density and porosity on sediment and contaminant transport. In *The role of erosion and sediment transport in nutrient and contaminant transfer*. JAHS Publ. 263.

Druine, F., Verney, R., Deloffre, J., Lemoine, J. P., Chapalain, M., Landemaine, V., & Lafite, R. (2018). In situ high frequency long term measurements of suspended sediment concentration in a turbid estuarine system (Seine Estuary, France): Optical turbidity sensors response to suspended sediment characteristics. *Marine Geology*, *400*, 24–37. https://doi.org/10.1016/j.margeo.2018.03.003

Dyer, K. R. (1989). Sediment processes in estuaries: Future research requirements. *Journal of Geophysical Research*, *94*(C10), 14327–14339. https://doi.org/10.1029/JC094iC10p14327

Eisma, D. (1991). Particle size of suspended matter in estuaries. *Geo-Marine Letters*, *11*(3–4), 147–153. https://doi.org/10.1007/bf02431001

Eisma, D. (1993). *Suspended matter in the aquatic environment*. Springer.

Fennessy, M. J., Dyer, K. R., & Huntley, D. A. (1994). INSSEV: An instrument to measure the size and settling velocity of flocs in situ. *Marine Geology*, *117*(1–4), 107–117. https://doi.org/10.1016/0025-3227(94)90009-4

Fennessy, M. J., Dyer, K. R., Huntley, D. A., & Bale, A. J. (1997). Estimation of settling flux spectra in estuaries using INSSEV. In N. Burt, R. Parker, & J. Watts (Eds.), *Cohesive sediments*. Wiley.

Fettweis, M. (2008). Uncertainty of excess density and settling velocity of mud flocs derived from in situ measurements. *Estuarine, Coastal and Shelf Science*, *78*(2), 426–436. https://doi.org/10.1016/j.ecss.2008.01.007

Fettweis, M., & Baeye, M. (2015). Seasonal variation in concentration, size, and settling velocity of muddy marine flocs in the benthic boundary layer. *Journal of Geophysical Research: Oceans*, *120*(8), 5648–5667. https://doi.org/10.1002/2014JC010644

Fettweis, M., Riethmüller, R., Verney, R., Becker, M., Backers, J., Baeye, M., et al. (2019). Uncertainties associated with in situ high-frequency long-term observations of suspended particulate matter concentration using optical and acoustic sensors. *Progress in Oceanography*, *178*, 102162. https://doi.org/10.1016/j.pocean.2019.102162

Fox, J. M., Hill, P. S., Milligan, T. G., Ogston, A. S., & Boldrin, A. (2004). Floc fraction in the waters of the Po River prodelta. *Continental Shelf Research*, *24*(15), 1699–1715. https://doi.org/10.1016/j.csr.2004.05.009

Franck, K. (1973). Flocculation of suspended sediment in the sea. *Nature*, *246*(5432), 348–350. https://doi.org/10.1038/246348a0

Fugate, D. C., & Friedrichs, C. T. (2003). Controls on suspended aggregate size in partially mixed estuaries. *Estuarine, Coastal and Shelf Science*, *58*(2), 389–404. https://doi.org/10.1016/S0272-7714(03)00107-0

Giovannoli, F. (1990). Horizontal transport and sedimentation by interflows and turbidity currents in Lake Geneva. In M. M. Tilzer & C. Serruya (Eds.), *Large lakes: Ecological structure and functions* (pp. 175–195). Springer. https://doi.org/10.1007/978-3-642-84077-7_9

Graham, G. W., Davies, E. J., Nimmo-Smith, W. A. M., Bowers, D. G., & Braithwaite, K. M. (2012). Interpreting LISST-100X measurements of particles with complex shape using digital in-line holography. *Journal of Geophysical Research*, *117*(C5), C05034. https://doi.org/10.1029/2011JC007613

Graham, G. W., & Nimmo-Smith, W. A. M. (2010). The application of holography to the analysis of size and settling velocity of suspended cohesive sediments. *Limnology and Oceanography: Methods*, *8*, 1–15. https://doi.org/10.4319/lom.2010.8.1

Gratiot, N., Bildsen, A., Tuan Anh, T., Thoss, H., Denis, H., Michallet, H., & Apel, H. (2017). Sediment flocculation in the Mekong River estuary, Vietnam, an important driver of geomorphological changes. *Comptes Rendus Geoscience*, *349*(6–7), 260–268. https://doi.org/10.1016/j.crte.2017.09.012

Gregory, J. (2013). Flocculation measurement techniques. In T. Tadros (Ed.), *Encyclopedia of colloid and interface science*. Springer. https://doi.org/10.1007/978-3-642-20665-8_172

Guerra, M., & Thomson, J. (2017). Turbulence measurements from five-beam acoustic Doppler current profilers. *Journal of Atmospheric and Oceanic Technology*, *34*(6), 1267–1284. https://doi.org/10.1175/JTECH-D-16-0148.1

Hawley, N. (1982). Settling velocity distribution of natural aggregates. *Journal of Geophysical Research*, *12*(C12), 9489–9498. https://doi.org/10.1029/JC087iC12p09489

Hetland, R. D. (2010). The effects of mixing and spreading on density in near-field river plumes. *Dynamics of Atmospheres and Oceans*, *49*, 37–53. https://doi.org/10.1016/s9999-9994(08)20541-6

Hill, P. S., Syvitski, J. P., Cowan, E. A., & Powell, R. D. (1998). In situ observations of floc settling velocities in Glacier Bay, Alaska. *Marine Geology*, *145*(1–2), 85–94. https://doi.org/10.1016/S0025-3227(97)00109-6

Hodder, K. R., & Gilbert, R. (2007). Evidence for flocculation in glacier-fed Lillooet Lake, British Columbia. *Water Research*, *41*(12), 2748–2762. https://doi.org/10.1016/j.watres.2007.02.058

Hodder, R. K. (2009). Flocculation: A key process in the sediment flux of a large, glacier-fed lake. *Earth Surface Processes and Landforms*, *34*(8), 1151–1163. https://doi.org/10.1002/esp.1807

Ishiguro, N., & Balvay, G. (2003). L'écoulement des eaux du Rhône dans le lac Léman. *Archives des Sciences*, *56*, 117–126. https://doi.org/10.5169/seals-740434

Izquierdo-Ayala, K., Garcia-Aragon, J. A., Castillo-Uzcanga, M. M., & Salinas-Tapia, H. (2021). Freshwater flocculation dependence on turbulence properties in the Usumacinta River. *Journal of Hydraulic Engineering*, *147*(12). https://doi.org/10.1061/(asce)hy.1943-7900.0001940

Jarvis, P., Jefferson, B., Gregory, J., & Parsons, S. A. (2005). A review of floc strength and breakage. *Water Research*, *39*(14), 3121–3137. https://doi.org/10.1016/j.watres.2005.05.022

Jarvis, P., Jefferson, B., & Parsons, S. A. (2005). Measuring floc structural characteristics. *Reviews in Environmental Science and Biotechnology*, *4*(1–2), 1–18. https://doi.org/10.1007/s11157-005-7092-1

Kolmogorov, A. N. (1941). Dissipation of energy in the locally isotropic turbulence. *Doklady Akademii Nauk SSSR*, *30*, 301–305. https://doi.org/10.1098/rspa.1991.0076

Kranenburg, C. (1999). Effects of floc strength on viscosity and deposition of cohesive sediment suspensions. *Continental Shelf Research*, *19*(13), 1665–1680. https://doi.org/10.1016/S0278-4343(98)00095-8

Kuprenas, R., Tran, D., & Strom, K. (2018). A shear-limited flocculation model for dynamically predicting average flocs size. *Journal of Geophysical Research: Oceans*, *123*(9), 6736–6752. https://doi.org/10.1029/2018JC014154

Lafite, R. (1990). *Caractérisation et dynamique des particules en suspension dans un domaine marin macrotidal influence par un estuaire: l'exemple de la Baie de Seine orientale (France)* (p. 294). Université de Rouen. Retrieved from https://www.theses.fr/1990ROUES007

Lee, B. J., Toorman, E., & Fettweis, M. (2014). Multimodal particle size distributions of fine-grained sediments: Mathematical modelling and field investigation. *Ocean Dynamics*, *64*(3), 429–441. https://doi.org/10.1007/s10236-014-0692-y

Li, X. C., Zhang, J. J., & Lee, J. H. W. (2004). Modelling particle size distribution dynamics in marine waters. *Water Research*, *38*(5), 1305–1317. https://doi.org/10.1016/j.watres.2003.11.010

Lick, W., Huang, H., & Jespen, R. (1993). Flocculation of fine-grained sediments due to differential settling. *Journal of Geophysical Research*, *98*, 10229–10288. https://doi.org/10.1029/93JC00519

Lick, W., & Lick, J. (1988). Aggregation and disaggregation of fine-grained lake sediments. *Journal of Great Lakes Research*, *14*(4), 514–523. https://doi.org/10.1016/S0380-1330(88)71583-X

Liu, J., Shen, Y., & Wang, X. (2022). Flocculation properties of cohesive fine-grained sediment in the Three Gorges Reservoir under variable turbulent shear. *Journal of Mountain Science*, *19*(8), 2286–2296. https://doi.org/10.1007/s11629-021-7079-6

Livsey, D. N., Crosswell, J. R., Turner, R. D. R., Steven, A. D. L., & Grace, P. R. (2022). Flocculation of riverine sediment draining to the Great Barrier Reef, implications for monitoring and modeling of sediment dispersal across continental shelves. *Journal of Geophysical Research: Oceans*, *127*(7), e2021JC017988. https://doi.org/10.1029/2021JC017988

Loizeau, J.-L., Girardclos, S., & Dominik, J. (2012). Taux d'accumulation de sédiments récents et bilan de matière particulaire dans le Léman (Suisse-France). *Archives des Sciences*, *65*, 81–92.

Lumley, J., & Terray, E. (1983). Kinematics of turbulence convected by a random wave field. *Journal of Physical Oceanography*, *13*(11), 2000–2007. https://doi.org/10.1175/1520-0485(1983)013<2000:KOTCBA>2.0.CO;2

Maggi, F., Manning, A. J., & Winterwerp, J. C. (2006). Image separation and geometric characterisation of mud flocs. *Journal of Hydrology*, *326*(1–4), 325–348. https://doi.org/10.1016/j.jhydrol.2005.11.005

Maggi, F., & Winterwerp, J. C. (2004). Method for computing the three-dimensional capacity dimension from two-dimensional projections of fractal aggregates. *Physical Review E*, *69*(1), 011405. https://doi.org/10.1103/physreve.69.011405

Manning, A. J., & Dyer, K. R. (1999). A laboratory examination of floc characteristics with regard to turbulent shearing. *Marine Geology*, *160*(1–2), 147–170. https://doi.org/10.1016/S0025-3227(99)00013-4

Manning, A. J., & Dyer, K. R. (2002). The use of optics for the in situ determination of flocculated mud characteristics. *Journal of Optics A: Pure and Applied Optics*, *4*, S71–S81. https://doi.org/10.1088/1464-4258/4/4/366

Manning, A. J., Dyer, K. R., Lafite, R., & Mikeš, D. (2004). Flocculation measured by video based instruments in the Gironde estuary during the European Commission SWAMIEE Project. *Journal of Coastal Research*, *41*, 59–69.

Many, G., Bourrin, F., Durrieu de Madron, X., Pairaud, I., Gangloff, A., Doxaran, D., et al. (2016). Particle assemblage characterization in the Rhone River ROFI. *Journal of Marine Systems*, *157*, 39–51. https://doi.org/10.1016/j.jmarsys.2015.12.010

Many, G., Durrieu de Madron, X., Verney, R., Bourrin, F., Renosh, P. R., Jourdin, F., & Gangloff, A. (2019). Geometry, fractal dimension and settling velocity of flocs during flooding conditions in the Rhône ROFI. *Estuarine, Coastal and Shelf Science*, *219*, 1–13. https://doi.org/10.1016/j.ecss.2019.01.017

Mari, X., Torréton, J. P., Trinh, C. B. T., Chu, V. T., Lefebvre, J. P., & Ouillon, S. (2011). Seasonal aggregation dynamics along a salinity gradient in the Bach Dang Estuary, North Vietnam. *Estuarine, Coastal and Shelf Science*, *96*, 151–158. https://doi.org/10.1016/j.ecss.2011.10.028

McCave, I. N. (1975). Vertical flux of particles in the ocean. *Deep-Sea Research*, *22*(7), 491–502. https://doi.org/10.1016/0011-7471(75)90022-4

McConnachie, J. L., & Petticrew, E. L. (2006). Tracing organic matter sources in riverine suspended sediment: Implications for fine sediment transfers. *Geomorphology*, *79*(1–2), 13–26. https://doi.org/10.1016/j.geomorph.2005.09.011

Mehta, A. J. (2022). *An introduction to hydraulics of fine sediment transport*. World Scientific. https://doi.org/10.1142/12873

Mietta, F., Chassagne, C., & Winterwerp, J. (2009). Shear-induced flocculation of a suspension of kaolinite as function of pH and salt concentration. *Journal of Colloid and Interface Science*, *336*(1), 134–141. https://doi.org/10.1016/j.jcis.2009.03.044

Mikeš, D., & Manning, A. J. (2010). Assessment of flocculation kinetics of cohesive sediments from the Seine and Gironde estuaries, France, through laboratory and field studies. *Journal of Waterway, Port, Coastal, and Ocean Engineering*, *136*(6), 306–318. https://doi.org/10.1061/(ASCE)WW.1943-5460.0000053

Mikeš, D., Verney, R., Lafite, R., & Belorgey, M. (2004). Controlling factors in estuarine flocculation processes: Experimental results with material from the Seine Estuary, Northwestern France. *Journal of Coastal Research*, *41*, 82–89.

Mikkelsen, A. O., Jones, S. E., Krivtsov, V., Mitchelson-Jacob, G., Jago, C. F., Jones, S. E., et al. (2008). The influence of schlieren on in situ optical measurements used for particle characterization. *Limnology and Oceanography: Methods*, *6*(3), 133–143. https://doi.org/10.4319/lom.2008.6.133

Mikkelsen, O. A., Hill, P. S., & Milligan, T. G. (2006). Single-grain, microfloc and macrofloc volume variations observed with a LISST-100 and a digital floc camera. *Journal of Sea Research*, *55*(2), 87–102. https://doi.org/10.1016/j.seares.2005.09.003

Mikkelsen, O. A., & Pejrup, M. (2001). The use of a LISST-100 laser particle sizer for in situ estimates of flocs size, density and settling velocity. *Geo-Marine Letters*, *20*(4), 187–195. https://doi.org/10.1007/s003670100064

Nghiem, J. A., Fischer, W. W., Li, G. K., & Lamb, M. P. (2022). A mechanistic model for mud flocculation in freshwater rivers. *Journal of Geophysical Research: Earth Surface*, *127*(5), e2021JF006392. https://doi.org/10.1029/2021JF006392

O'Connor, D. J. (1988). Models of sorptive toxic substances in freshwater systems. III Streams and Rivers. *Journal of Environmental Engineering*, *114*(3), 552–574. https://doi.org/10.1061/(ASCE)0733-9372(1988)114:3(552)

O'Melia, C. R., & Tiller, C. L. (1993). Physicochemical aggregation and deposition in aquatic environments. In J. Buffle & H. P. van Leewen (Eds.), *Environmental particles* (Vol. 2). Lewis Publishers.

Osborn, R., Dillon, B., Tran, D., Abolfazli, E., Dunne, K. B. J., Nittrouer, J. A., & Strom, K. (2021). FlocARAZI: An in-situ, image-based profiling instrument for sizing solid and flocculated suspended sediment. *Journal of Geophysical Research: Earth Surface*, *126*(11), e2021JF006210. https://doi.org/10.1029/2021JF006210

Osborn, R., Dunne, K. B. J., Ashley, T., Nittrouer, J. A., & Strom, K. (2023). The flocculation state of mud in the lowermost freshwater reaches of the Mississippi River: Spatial distribution of sizes, seasonal changes, and their impact on vertical concentration profiles. *Journal of Geophysical Research: Earth Surface*, *128*(7), e2022JF006975. https://doi.org/10.1029/2022JF006975

Pejrup, M., & Mikkelsen, O. A. (2010). Factors controlling the field settling velocity of cohesive sediments in estuaries. *Estuarine, Coastal and Shelf Science*, *87*(2), 177–185. https://doi.org/10.1016/j.ecss.2009.09.028

Piton, V., Lemmin, U., Bourrin, F., Wynn, H. K., Kinschi, V., & Barry, D. A. (2023a). CTD, LISST-100X and Signature1000 data for "From particles to flocs: Revealing where flocculation occurs in the nearfield of a negatively-buoyant river plume in a large lake (Lake Geneva)" [Dataset]. Zenodo. https://doi.org/10.5281/zenodo.7773589

Piton, V., Lemmin, U., Bourrin, F., Wynn, H. K., Kinschi, V., & Barry, D. A. (2023b). LISST-HOLO images and files for "From particles to flocs: Revealing where flocculation occurs in the nearfield of a negatively-buoyant river plume in a large lake (Lake Geneva)" [Dataset]. Zenodo. https://doi.org/10.5281/zenodo.7773542

Piton, V., Soulignac, F., Lemmin, U., Graf, B., Wynn, H. K., Blanckaert, K., & Barry, D. A. (2022). Tracing unconfined nearfield spreading of a river plume interflow in a large lake (Lake Geneva): Hydrodynamics, suspended particulate matter and associated fluxes. *Frontiers in Water*, *4*, 943242. https://doi.org/10.3389/frwa.2022.943242

Rasmussen, P. P., Gray, J. R., Glysson, G. D., & Ziegler, A. C. (2009). Guidelines and procedures for computing time-series suspended-sediment concentrations and loads from in-stream turbidity-sensor and streamflow data. *U.S. Geological Survey Techniques and Methods Book 3* (p. 53). chapter C4.

Sehgal, D., Martínez-Carreras, N., Hissler, C., Bense, V. F., & Hoitink, A. J. F. (2022). A genericrelation between turbidity, suspended particulate matter concentration, and sediment characteristics. *Journal of Geophysical Research: Earth Surface*, *127*(12), e2022JF006838. https://doi.org/10.1029/2022JF006838

Silva, T. A., Girardclos, S., Stutenbecker, L., Bakker, M., Costa, A., Schlunegger, F., et al. (2019). The sediment budget and dynamics of a delta-canyon-lobe system over the Anthropocene timescale: The Rhone River delta, Lake Geneva (Switzerland/France). *Sedimentology*, *66*(3), 838–858. https://doi.org/10.1111/sed.12519

Slattery, M. C., & Burt, T. P. (1997). Particle size characteristics of suspended sediment in hillslope runoff and stream flow. *Earth Surface Processes and Landforms*, *22*(8), 705–719. https://doi.org/10.1002/(SICI)1096-9837(199708)22:8<705::AID-ESP739>3.0.CO;2-6

Soulignac, F., Lemmin, U., Hamze-Ziabari, S. M., Wynn, H. K., Graf, B., & Barry, D. A. (2021). Rapid changes in river plume dynamics caused by advected wind-driven coastal upwelling as observed in Lake Geneva. *Limnology & Oceanography*, *66*(8), 3116–3133. https://doi.org/10.1002/lno.11864

Sreenivasan, K. (1995). On the universality of the Kolmogorov constant. *Physics of Fluids*, *7*(11), 2778–2784. https://doi.org/10.1063/1.868656

Strom, K., & Keyvani, A. (2011). An explicit full-range settling velocity equation for mud flocs. *Journal of Sedimentary Research*, *81*(12), 921–934. https://doi.org/10.2110/jsr.2011.62

Strom, K., & Keyvani, A. (2016). Flocculation in a decaying shear field and its implications for mud removal in near-field river mouth discharge. *Journal of Geophysical Research: Oceans*, *121*(4), 2142–2162. https://doi.org/10.1002/2015JC011169

Styles, R. (2006). Laboratory evaluation of the LISST in a stratified fluid. *Marine Geology*, *227*(1–2), 151–162. https://doi.org/10.1016/j.margeo.2005.11.011

Thill, A., Veerapaneni, S., Simon, B., Wiesner, M., Bottero, J. Y., & Snidaro, D. (1998). Determination of structure of aggregates by confocal scanning laser microscopy. *Journal of Colloid and Interface Science*, *204*(2), 357–362. https://doi.org/10.1006/jcis.1998.5570

Thonon, I., Roberti, J. R., Middelkoop, H., van der Perk, M., & Burrough, P. A. (2005). In situ measurements of sediment settling characteristics in floodplains using a LISST-ST. *Earth Surface Processes and Landforms*, *30*(10), 1327–1343. https://doi.org/10.1002/esp.1239

Tran, D., & Strom, K. (2017). Suspended clays and silts: Are they independent of dependent fractions when it comes to settling in a turbulent suspension? *Continental Shelf Research*, *138*, 81–94. https://doi.org/10.1016/j.csr.2017.02.011

Tsai, C. H., Iacobellis, S., & Lick, W. (1987). Flocculation of fine-grained lake sediments due to a uniform shear stress. *Journal of Great Lakes Research*, *13*(2), 135–146. https://doi.org/10.1016/S0380-1330(87)71637-2

Udden, J. A. (1914). Mechanical composition of clastic sediments. *Geological Society of America Bulletin*, *25*(1), 655–744. https://doi.org/10.1130/GSAB-25-655

Vahedi, A., & Gorczyca, B. (2011). Application of fractal dimensions to study the structure of flocs formed in lime softening process. *Journal of Water Resources*, *45*(2), 545–556. https://doi.org/10.1016/j.watres.2010.09.014

van Leussen, W. (1997). The Kolmogorov microscale as a limiting value for the floc size of suspended fine grained sediments in estuaries. In N. Burt, R. Parker, & J. Watts (Eds.), *Cohesive sediment* (pp. 45–62). Wiley.

van Leussen, W., & Cornelisse, J. M. (1994). The determination of the sizes and settling velocities of estuarine flocs by an underwater video system. *Journal of Sea Research*, *31*, 231–241. https://doi.org/10.1016/0077-7579(93)90024-M

Verney, R., Lafite, R., & Brun-Cottan, J. C. (2009). Flocculation potential of estuarine particles: The importance of environmental factors and of the spatial and seasonal variability of suspended particulate matter. *Estuaries and Coasts*, *32*(4), 678–693. https://doi.org/10.1007/s12237-009-9160-1

Wentworth, C. K. (1922). A scale of grade and class terms for clastic sediments. *The Journal of Geology*, *30*(5), 377–392. https://doi.org/10.1086/622910

Wheatland, J. A. T., Spencer, K. L., Droppo, I. G., Carr, S. J., & Bushby, A. J. (2020). Development of novel 2D and 3D correlative microscopy to characterise the composition and multiscale structure of suspended sediment aggregates. *Continental Shelf Research*, *200*, 104112. https://doi.org/10.1016/j.csr.2020.104112

Winterwerp, J. C. (1998). A simple model for turbulence induced flocculation of cohesive sediment. *Journal of Hydraulic Research*, *36*(3), 309–326. https://doi.org/10.1080/00221689809498621

Winterwerp, J. C. (1999). *On the dynamics of high-concentrated mud suspensions* (PhD thesis) (p. 172). TU Delft.

Winterwerp, J. C. (2002). On the flocculation and settling velocity of estuarine mud. *Continental Shelf Research*, *22*(9), 1339–1360. https://doi.org/10.1016/S0278-4343(02)00010-9

Winterwerp, J. C., Manning, A., Martens, C., De Mulder, T., & Vanlede, J. (2006). A heuristic formula for turbulence-induced flocculation of cohesive sediment. *Estuarine, Coastal and Shelf Science*, *68*(1–2), 195–207. https://doi.org/10.1016/j.ecss.2006.02.003

Woodward, J., Porter, P., Lowe, A., Walling, D., & Evans, A. (2002). Composite suspended sediment particles and flocculation in glacial meltwaters: Preliminary evidence from Alpine and Himalayan basins. *Hydrological Processes*, *16*(9), 1735–1744. https://doi.org/10.1002/hyp.361

Woodward, J., & Walling, D. (2007). Composite suspended sediment particles in river systems: Their incidence, dynamics and physical characteristics. *Hydrological Processes*, *21*(26), 3601–3614. https://doi.org/10.1002/hyp.6586

Xu, C., Odum, B., Chen, Y., & Yao, P. (2022). Evaluation of the role of silt content on the flocculation behavior of clay-silt mixtures. *Water Resources Research*, *58*(11), e2021WR030964. https://doi.org/10.1029/2021WR030964

Zahner, P., & Vernet, J.-P. (1984). Dynamique du système lacustre. In *Commission Internationale pour la Protection des Eaux du Léman (CIPEL). Le Léman Synthèse 1957–1982* (pp. 55–63).

Zhang, J., Shen, X., Zhang, Q., Maa, J. P. Y., & Lin, M. (2022). Role of gravity in coagulation of colloidal particles under low-shear environments. *Marine Geology*, *449*, 106822. https://doi.org/10.1016/j.margeo.2022.106822

References From the Supporting Information

Aminot, A., & Kérouel, R. (2004). *Hydrologie des écosystèmes marins: Paramètres et analyses* (p. 336). Ifremer.

Davies, E. J., Buscombe, D., Graham, G. W., & Nimmo-Smith, W. A. M. (2015). Evaluating unsupervised methods to size and classify suspended particles using digital in-line holography. *Journal of Atmospheric and Oceanic Technology*, *32*(6), 1241–1256. https://doi.org/10.1175/JTECH-D-14-00157.1

Deines, K. L. (1999). Backscatter estimation using broadband acoustic Doppler current profilers. In *Proceedings of the IEEE 6th Working Conference on Current Measurement (Cat. No.99CH36331), San Diego, California, USA, 13 March 1999*. https://doi.org/10.1109/CCM.1999.755249

François, R. E., & Garrison, G. R. (1982). Sound absorption based on ocean measurements. Part II: Boric acid contribution and equation of total absorption. *Journal of the Acoustical Society of America*, *72*(6), 1879–1890. https://doi.org/10.1121/1.388673

Lee, C., & Kramer, T. A. (2004). Prediction of three-dimensional fractal dimensions using the two-dimensional properties of fractal aggregates. *Advances in Colloid and Interface Science*, *112*(1–3), 49–57. https://doi.org/10.1016/j.cis.2004.07.001

Mikkelsen, O. A., Hill, P. S., Milligan, T. G., & Chant, R. J. (2005). In situ particle size distributions and volume concentrations from a LISST-100 laser particle sizer and a digital floc camera. *Continental Shelf Research*, *25*(16), 1959–1978. https://doi.org/10.1016/j.csr.2005.07.001

Mikkelsen, O. A., & Pejrup, M. (2000). In situ particle size spectra and density of particle aggregates in a dredging plume. *Marine Geology*, *170*(3–4), 443–459. https://doi.org/10.1016/S0025-3227(00)00105-5

Mullison, J. (2017). Backscatter estimation using broadband acoustic Doppler current profilers-updated. In *Proceedings of the ASCE Hydraulic Measurements & Experimental Methods Conference, Durham, NH, USA, 9–12 July*. Retrieved from http://www.teledynemarine.com/Documents/Brand%20Support/RD%20INSTRUMENTS/Technical%20Resources/Technical%20Notes/WorkHorse%20-%20ADCP%20Special%20Applications%20and%20Modes/FSA031.pdf

Owen, R. B., & Zozulya, A. A. (2000). In-line digital holographic sensor for monitoring and characterizing marine particulates. *Optical Engineering*, *39*(8), 2187–2197. https://doi.org/10.1117/1.1305542

Spicer, P. T., & Pratsinis, S. E. (1996). Shear-induced flocculation: The evolution of floc structure and the shape of the size distribution at steady state. *Water Research*, *30*(5), 1049–1056. https://doi.org/10.1016/0043-1354(95)00253-7

Tessier, C. (2006). *Caractérisation et dynamique des turbidités en zone côtière: L'exemple de la région marine Bretagne Sud* (PhD thesis). Université de Bordeaux 1. Retrieved from https://archimer.ifremer.fr/doc/2006/these-2325.pdf